Altered Expression of Cadherin-8 and Cadherin-11 in Neural Circuit Development: Implications for Autism

Jeannine A. Frei[1,*], Robert F. Niescier[1], Morgan S. Bridi[1], Madel Durens[1], Jonathan E. Nestor[1], Xiaobing Yuan[2], Derek M. Dykxhoorn[3], Michael W. Nestor[1], Shiyong Huang[1], Gene J. Blatt[1], and Yu-Chih Lin[1,*]

[1]Program in Neuroscience, Hussman Institute for Autism, Baltimore, MD, USA

[2]East China Normal University, Shanghai, China

[3]John P. Hussman Institute for Human Genomics, University of Miami Miller School of Medicine, Miami, FL, USA

***Correspondence:**

Jeannine A. Frei
jfrei@hussmanautism.org
Yu-Chih Lin
yclin@hussmanautism.org

Keywords: cadherin-8, cadherin-11, Cdh11 knockout mice, autism spectrum disorder, neuroligin-1, dendrite, synapse, induced pluripotent stem cells

Number of words: 7894

Number of figures: 6

Abstract

Autism spectrum disorder (ASD) is a neurological condition characterized by difficulties in social interaction, communication, and behavior. The classical type II cadherins cadherin-8 (Cdh8, CDH8) and cadherin-11 (Cdh11, CDH11) have been implicated as autism risk gene candidates. To explore the role of cadherins in the etiology of autism, we investigated their expression patterns during mouse brain development and analyzed their functions using *Cdh11* knockout mice. Expression of cadherin-8 and cadherin-11 was developmentally regulated and enriched in cortex, hippocampus, and thalamus/striatum during the peak of dendrite formation and synaptogenesis. Cadherin-8 preferentially localized to excitatory synapses where it interacted with neuroligin-1. Levels of cadherin-8, neuroligin-1, and PSD-95 were all significantly increased in *Cdh11* knockout brains. Additionally, *Cdh11*$^{-/-}$ hippocampal neurons exhibited increased dendritic complexity along with altered neuronal and synaptic activity. Similar to the expression profiles in *Cdh11* knockout mice, induced pluripotent stem cell (iPSC)-derived cortical neural precursor cells (NPCs) and cortical organoids generated from individuals with autism showed elevated CDH8 expression levels while CDH11 expression levels were decreased. Together, these results strongly suggest that cadherin-8 and cadherin-11 are involved in regulating the development of neuronal circuitry and that alterations in the expression levels of cadherin-8 and cadherin-11 may contribute to the etiology of autism.

Introduction

Autism is a neurodevelopmental condition characterized by marked qualitative changes in social interaction, communication, and behavior (American Psychiatric Association, 2013). Current estimates indicate that 1 in 59 children in the United States are affected (Baio et al., 2018). Autism is characterized by both phenotypic and genetic heterogeneity. This genetic complexity is illustrated by the fact that no single gene associated with the condition contributes to more than 1% of the autism cases (Huguet, Ey, & Bourgeron, 2013; Jeste & Geschwind, 2014). Nevertheless, many of the genes implicated in the condition encode for synaptic cell adhesion molecules, scaffolding proteins and cytoskeletal regulators (Betancur, Sakurai, & Buxbaum, 2009; Bourgeron, 2015; Lin, Frei, Kilander, Shen, & Blatt, 2016). These autism risk genes converge into distinct cellular pathways that appear to be commonly affected, including neurite outgrowth, dendritic spine stability, synaptogenesis, and synaptic function (Betancur et al., 2009; Bourgeron, 2015; Chen, Yu, Fu, & Li, 2014; Hussman et al., 2011; Joensuu, Lanoue, & Hotulainen, 2017; Lin et al., 2016).

One large group of synaptic cell adhesion molecules, the cadherin superfamily, has been widely associated with neurodevelopmental disorders, including autism (Lin et al., 2016; Redies, Hertel, & Hübner, 2012). The cadherin family comprises more than one hundred members, which are further divided into subfamilies, including classical type I and II cadherins, clustered and non-clustered protocadherins, and atypical FAT cadherins (Hirano & Takeichi, 2012; Hulpiau & van Roy, 2009). Multiple studies have identified cadherins across all subfamilies as candidate risk genes for autism (Camacho et al., 2012; Chapman et al., 2011; Crepel et al., 2014; Cukier et al., 2014; Depienne et al., 2009; Girirajan et al., 2013; Hussman et al., 2011; Kenny et al., 2014; Marshall et al., 2008; Morrow et al., 2008; Neale et al., 2012; O'Roak et al., 2012; Pagnamenta et al., 2011; Sanders et al., 2011; van Harssel et al., 2013; K. Wang et al., 2009; Willemsen et al., 2010). The most-well studied classical type I cadherin, N-cadherin, is broadly expressed in the central nervous system and has been implicated in multiple processes during nervous system development (Arikkath & Reichardt, 2008; Friedman, Benson, & Huntley, 2015; Hirano & Takeichi, 2012; Seong, Yuan, & Arikkath, 2015; Takeichi & Abe, 2005). In contrast to classical type I cadherins, the expression profile of classical type II cadherins is more restricted to specific brain circuits and subcellular compartments (Inoue, Tanaka, Suzuki, & Takeichi, 1998; Korematsu & Redies, 1997; Suzuki, Inoue, Kimura, Tanaka, & Takeichi, 1997; C. Wang, Pan, Wang, Blatt, & Yuan, 2019). The differential expression patterns of classical type II cadherins allow them to confer sophisticated synaptic specificity (Basu, Taylor, & Williams, 2015).

The aim of the current study was to understand the involvement of classical type II cadherins in autism and to decipher potential cellular mechanisms mediated by these cadherins. We focused our study on the classical type II cadherins cadherin-8 (Cdh8, CDH8) and cadherin-11 (Cdh11, CDH11) as these specific cadherins have been identified as autism risk genes in a genome-wide association study and by whole exome sequencing (Hussman et al., 2011, Cukier et al., 2014). In addition, other studies have identified rare mutations and SNP variants in *CDH8* and *CDH11* genes, respectively, in individuals with autism (Pagnamenta et al., 2011, 2008, Crepel et al., 2014). Here, we first examined the expression profiles and binding partners of cadherin-8 and cadherin-11 in developing mouse brains. The results indicated that these two cadherins engage in different cellular pathways. We further used the *Cdh11* knockout mouse to identify potential mechanisms altered in autism as levels of these two cadherins were differentially altered in human induced pluripotent stem cell (hiPSC)-derived neural precursor cells (NPCs) and organoids

generated from individuals with autism. These data suggested that a shift in the balance between cadherin-8 and cadherin-11 causes altered neural circuit formation that may drive aspects of autism pathophysiology.

Materials and Methods

Animals

C57BL/6 mice were purchased from the animal facility of the University of Maryland School of Medicine Program in Comparative Medicine (Baltimore, MD, USA). *Cdh11*^{tm1Mta}/HensJ mice were purchased from the Jackson Lab (Horikawa, Radice, Takeichi, & Chisaka, 1999). Mice were housed and cared for by the AAALAC accredited program of the University of Maryland School of Medicine. Female mice were group-housed and male mice were singly housed with *ad libitum* food and water accessibility under a standard 12-hour light/dark cycle. Neonatal mice of both sexes were euthanized for the preparation of neuronal and glial cultures. To match the mixed-gender condition in cultures animals of both sexes were used for biochemistry. All experiments were reviewed and approved by the Institutional Care and Use Committees (IACUC) of the University of Maryland School of Medicine and the Hussman Institute for Autism, and were performed in accordance with the animal care guidelines of the National Institute of Health.

Antibodies

The antibodies used in this study are listed in Table 1. The specificity of the antibodies was carefully examined prior to conducting the experiments (Supplementary Figure 1).

Plasmids

Myc-flag-tagged full-length *Cdh8* was purchased from Origene (plasmid #MR218916). *Cdh8* was expressed under the CMV promoter in the pCMV6 vector. Flag-tagged full-length *Cdh11* was expressed under the EF-1α promotor in the pBos vector (gift from Dr. Megan Williams, University of Utah, USA). HA-tagged *Nlgn1* plasmid was a gift from Peter Scheiffele (Addgene plasmid # 15260; RRID:Addgene_15260) (Chih, Gollan, & Scheiffele, 2006). *Nlgn1* was expressed under the chicken β-actin promotor in the pCAAGs vector. pLL3.7-GFP was a gift from Luk Parijs (Addgene plasmid # 11795; RRID:Addgene_11795) (Rubinson et al., 2003).

Cell cultures and transfection

Glial cell cultures were prepared from postnatal day 0 (P0) C57BL/6 mouse cortices and cultured in Dulbecco's MEM growth medium (Invitrogen Cat#11960044) supplemented with 10% FBS (Millipore Sigma Cat#F4135), 2 mM L-glutamine (Invitrogen Cat#25030081) and 1% penicillin/streptomycin (Invitrogen Cat#15140122). Primary neuronal cultures were prepared from P0 C57BL/6 mouse cortex (3-4 animals per culture) or hippocampus (8-10 animals per culture). Hippocampal cultures from *Cdh11*^{tm1Mta}/HensJ mice were prepared from individual pups at P0. The genotype of each pup was determined after the culture was prepared. Only *Cdh11* wild-type and knockout cultures were used for further experiments. In brief, brain tissue was dissected and meninges were removed. Tissue was digested in papain and cells were dissociated and plated on surfaces coated with 20 μg/ml poly-D-lysine (Millipore Sigma Cat#P6407). Cortical and hippocampal cultures were maintained in serum-free Neurobasal-A media (Invitrogen Cat#10888022) containing 2 mM L-glutamine (Gibco Cat#25030081), 1% penicillin/streptomycin

(Gibco Cat#15140122) and 2% B27 supplement (Gibco Cat#17504044). For Western blot analysis, glial cells were harvested at 14 days *in vitro* (DIV) and cortical neurons were harvested at different time points: 1, 3, 7 and 14 DIV. Neuro-2A (N2a, mouse neuroblastoma cell line; ATCC) cells were maintained in Dulbecco's MEM growth medium (Invitrogen Cat#11960044) supplemented with 10% FBS (Millipore Sigma Cat#F4135), 2 mM L-glutamine (Gibco Cat#25030081) and 1% penicillin/streptomycin (Gibco Cat#15140122). N2a cells were transfected with full-length plasmids using Lipofectamine 3000 (Invitrogen Cat#L3000015) according to the manufacturer's protocol. Cells were harvested 48 hours post-transfection.

Western blot analysis

At the indicated points in development, mice of both sexes were sacrificed and brains were quickly dissected. Either whole brains or different brain areas, including cortex, hippocampus, cerebellum and thalamus/striatum were collected. Brain tissue was snap-frozen in liquid nitrogen. All tissues and cells were lysed in RIPA buffer (Cell Signaling Technologies Cat# 9806S) supplemented with PMSF (Cell Signaling Technologies Cat#8553S) and protease and phosphatase inhibitor cocktail (Thermo Fisher Scientific Cat#78442). Protein concentration was determined using Pierce BCA protein assay kit (Thermo Fisher Scientific Cat#23227) and measured by the Tecan Spark 10M multimode microplate reader. Ten micrograms of protein samples from brain or cell lysates were run on 10% Tris-glycine SDS-PAGE gels and transferred to a PVDF membrane. Membranes were blocked in 5% milk/TBS-T followed by incubation of primary antibodies overnight and secondary HRP-coupled antibodies for one hour at room temperature. Blots were imaged with the ChemiDoc Touch Imaging System (Bio Rad; see Supplementary Figure 2 for full scans of original blots) and band densitometries were analyzed using the Image Lab software (Bio Rad). Intensities were normalized to either GAPDH or β-actin signals. Full scans of all blots

Synaptic fractionation

Synaptic plasma membrane (SPM) and postsynaptic density (PSD) fractions were prepared according to Bermejo et al. (Bermejo, Milenkovic, Salahpour, & Ramsey, 2014). In brief, brains of P21 mice were quickly removed and forebrain was dissected on ice. Brain tissues were homogenized in 0.32 M sucrose in 4 mM HEPES (pH 7.4) at 900 rpm with 12 strokes using a glass-Teflon tissue homogenizer. Removal of the nuclear fraction (P1) was achieved by low speed centrifugation at 900 x g for 10 minutes. The supernatant (S1) was collected and centrifuged at 10,000 x g for 15 minutes to yield crude synaptosomal fraction (P2) and cytosol/light membranes in the supernatant (S2). P2 pellet was lysed in ddH_2O by hypo-osmotic shock and centrifuged at 25,000 x g for 20 minutes to obtain pelleted synaptosomes (P3) and vesicular fraction (S3). The vesicular fraction was pelleted by ultracentrifugation at 165,000 x g for 2 hours. Synaptosomes (P3) were layered on top of a discontinuous sucrose gradient. Ultracentrifugation of the gradient at 150,000 x g for 2 hours yielded the SPM fraction. SPM was collected and pelleted by ultracentrifugation at 200,000 x g for 30 minutes. To prepare PSD fraction, SPM was incubated in 0.5% Triton-X100 for 15 minutes followed by centrifugation at 32,000 x g for 30 minutes. All centrifugation steps were performed at 4°C. Fractions were analyzed by Western blot and intensities of cadherin-8, cadherin-11 and PSD-95 positive signals in SPM and PSD fractions were normalized to the total protein input.

Co-immunoprecipitation

P14 forebrain and transfected and untransfected N2a cells were homogenized in lysis buffer containing 20 mM Tris, pH 7.5, 150 mM NaCl and 1% Triton X-100 supplemented with PMSF (Cell Signaling Technologies Cat#8553S) and protease and phosphatase inhibitor cocktail (Thermo Fisher Scientific Cat#78442). Protein extract (0.5 mg, standardized to 1 mg/ml) was precleared with 50 µl Protein G Sepharose 4 Fast Flow (Millipore Sigma Cat#GE17-0618-01) or rProtein A Sepharose Fast Flow (Millipore Sigma Cat#GE17-1279-01) for 1 hour at 4° C. Precleared supernatant was incubated with 2 µg anti-cadherin-8 (DSHB Cat#CAD8-1), 7 µg anti-cadherin-11 (Thermo Fisher Scientific Cat#32-1700) or 4 µg anti-HA antibodies (Millipore Sigma Cat#H6908), and mouse or rabbit IgGs for 2 hours at 4° C. Samples were precipitated with 50 µl of pre-equilibrated Protein G Sepharose 4 Fast Flow or rProtein A Sepharose Fast Flow for 1 hour at 4°C with gentle mixing. Immunoprecipitates were washed three times in lysis buffer and eluted by boiling in 50 µl sample buffer. Overexpressed myc-flag-tagged cadherin-8 was immunoprecipitated using the Pierce c-My-tag IP/Co-IP kit according to the manufacturer's protocol (Thermo Fisher Cat#23620). Co-immunoprecipitated proteins were determined by Western blot analysis.

Immunocytochemistry

Surface staining was performed on low-density hippocampal cultures (20,000 cells/2 cm^2) at 15 DIV. Cells were washed with artificial cerebrospinal fluid (aCSF) containing 124 mM NaCl, 5 mM KCl, 1.23 mM NaH_2PO_4, 26 mM $NaHCO_3$, 10 mM Dextrose, 1 mM $MgCl_2$, 1 mM $CaCl_2$, and supplemented with 10% BSA. Cells were incubated with aCSF containing primary antibody for one hour at 20°C. After washing with aCSF/10% BSA, cells were incubated with secondary antibody for one hour at 20°C before fixation with 4% paraformaldehyde for 15 minutes (Gu & Huganir, 2016; Noel et al., 1999). For total staining, N2a and primary cells were fixed with 4% paraformaldehyde, permeabilized with 0.1% Triton-X100 and incubated with primary antibodies overnight and secondary antibodies for one hour at room temperature. Cells were labeled with DAPI and coverslips were mounted on glass slides with ProLong Diamond antifade mounting solution (Thermo Fisher Scientific Cat#P36934) prior to imaging. Images were taken using a Zeiss LSM-780 scanning confocal microscope with a 40x objective/1.30 EC-plan-neofluar oil or a 63x objective/1.40 plan-apochromat oil for N2a cells, and a 63x objective/1.40 plan-apochromat oil and 4x zoom for primary cells. For co-localization analysis, cadherin-8-positive puncta were manually counted and classified as either co-localizing with PSD-95 or GAT-1 (partially or totally overlapping puncta), being adjacent to PSD-95 or GAT-1 (puncta that were in close proximity and touching each other) or cadherin-8 puncta that were PSD-95- or GAT-1-negative.

Direct stochastic optical reconstruction microscopy (dSTORM) imaging

67,000 cells prepared from P0 C57BL/6 mouse hippocampus were plated onto Fluorodish 35 mm dishes with 23 mm #1.5-glass bottoms (Cat# FD35-100). At 15 DIV, cells were surface stained with either cadherin-8 or neuroligin-1 primary antibody and Alexa647-conjugated secondary antibody as described above. After surface staining, cells were fixed, permeabilized and

immunostained with PSD-95 primary antibody and Alexa488-conjugated secondary antibody and maintained in PBS prior to imaging. Imaging was performed using a Nikon N-STORM microscope, using the following buffer system: 150 mM tris-HCl pH 8.0, 100 mM MEA-HCl (Millipore Sigma Cat#M6500), 3% Oxyfluor (Millipore Sigma Cat#SAE0059), and 2% DL-Lactate (Millipore Sigma Cat#L1375) (Nahidiazar, Agronskaia, Broertjes, van den Broek, & Jalink, 2016). A minimum of 20,000 frames were obtained using 100% laser power of 488 and 647 nm channels with 16 ms exposure time using elliptical lens for 3D analysis. STORM processing was performed using the Fiji (NIH) plug-in ThunderSTORM (Ovesný, Křížek, Borkovec, Svindrych, & Hagen, 2014). For nearest neighbor analysis, the ThunderSTORM CBC function was used to compare the cadherin-8 or neuroligin-1 localization tables to the corresponding PSD-95 table. Individual molecules of either cadherin-8 or neuroligin-1 were manually identified, and the closest molecule of PSD-95 was quantified. 50 fluorescence particles per image were examined, unless fewer than that were available for analysis. For a negative control, numbers between 0-400 were randomly generated using Microsoft Excel. For comparison between random, cadherin-8, and neuroligin-1, values were binned at 10 nm intervals and plotted using Graph Pad Prism 8 software (GraphPad Prism Software, RRID: SCR_002798).

Morphometric analysis

Cultured *Cdh11* wild-type and knockout hippocampal neurons (300,000 cells/2 cm^2) were transfected at 9 DIV with the pLL3.7-GFP vector (Addgene Cat#11795) using Lipofectamine 2000 (Invitrogen Cat#11668-019) and fixed at 15 DIV with 4% paraformaldehyde. Z-stack images were taken using Zeiss LSM-780 scanning confocal microscope with a 63x objective/1.40 plan-apochromat oil at 1500x1500 resolution and stitched with 2x2 frames. For dendritic spine analysis, two to three dendrite segments per neuron were randomly selected from primary, secondary and tertiary branches on the apical dendrite. The number of dendritic spines ($\leq$ 2 µm in length) was quantified using Fiji (NIH). For analysis of dendritic morphology, neurons were traced and the total dendrite length and branch tip number were quantified using Fiji (NIH) with NeuronJ plugin (Meijering et al., 2004). Neurons were further analyzed using Fiji (NIH) with Sholl analysis plugin (Ferreira et al., 2014). From the center of the cell body, concentric circles having 10 µm increments in radius were defined and the number of traced dendrites crossing each circle was quantified. The complexity of dendritic arbors was analyzed by the area under the curve (AUC) using Graph Pad Prism 8 software (GraphPad Prism Software, RRID: SCR_002798).

Calcium imaging

Cdh11 wild-type and knockout hippocampal neurons were seeded in triplicates at a density of 30,000 cells per well on a 96-well plate coated with 20 µg/ml poly-D-lysine (Millipore Sigma Cat#P6407). At 7 DIV neurons were infected with the IncuCyte NeuroBurst Orange lentivirus under a synapsin promotor (Essen Bioscience Sartorius Cat# 4736). After 24 hours, virus was removed by changing the media. Cells were imaged at 15 DIV for 24 hours using the IncuCyte S3 system (Essen Bioscience Sartorius Cat#4763). Using the IncuCyte S3 2019A software (Essen Bioscience Sartorius) the following parameters were calculated: number of active neurons, mean correlation of activity, mean burst strength, and mean burst rate. The total number of active neurons was identified by the analysis definition. For the mean correlation of activity the temporal pattern

of the change in fluorescent intensity for each active neuron was compared to every other active neuron in the image. A value between -1 and 1 was generated, with 0 being completely random (no correlation) and 1 being identical patterns of change in fluorescent intensity (highly correlated). Fisher r-to-z transformation was applied to assess the significance between correlation coefficients. The mean burst strength was analyzed by integrating the area under the curve divided by its duration. This value was calculated for each burst individually and then averaged for each active neuron, followed by averaging across the entire image. To calculate the mean burst rate the total number of bursts for each active neuron was divided by minutes of scan time, followed by averaging the values for all active neurons across the entire image. The total number of cells was obtained by counting DAPI-positive nuclei. IncuCyte NeuroLight Orange lentivirus (Essen Bioscience Sartorius Cat# 4758) was used to measure the infection rate of *Cdh11* wild-type and knockout hippocampal neurons. Neurons were infected at 7 DIV and the virus was removed after 24 hours by changing the media. Neurons were fixed with 4% paraformaldehyde at 16 DIV and imaged using Evos Auto 2.0 system (Invitrogen) with a 10x objective. The number of infected cells was counted and subsequently normalized to the total cell number determined by DAPI.

Electrophysiology

Electrophysiological recordings were conducted using *ex vivo* brain slices of *Cdh11* wild-type and knockout littermate mice between P21 and P24. Mice were anesthetized with isoflurane, decapitated, and brains removed into ice-cold sucrose cutting solution containing (in mM): 215 Sucrose, 2.5 KCl, 1.25 NaH_2PO4, 2.8 $NaHCO_3$, 7 Dextrose, 3 Na-Pyruvate, 1 Na-Ascorbate, 0.5 $CaCl_2$, 7 $MgCl_2$ (pH 7.4, bubbled with 95% CO_2/5% O_2). Near-horizontal slices containing hippocampus, 300 µm thick, were sectioned with a vibrating microtome (VT1200S, Leica Biosystems). After cutting, slices were transferred into a warmed recovery chamber filled with bubbled artificial cerebrospinal fluid (aCSF) containing the following (in mM): 125 NaCl, 2.5 KCl, 1.25 NaH_2PO4, 25 $NaHCO_3$, 25 Dextrose, 2 $CaCl_2$, 1 $MgCl_2$, 3 Na-Pyruvate, and 1 Na-Ascorbate. After recovering for 30 minutes at a temperature of 34°C, the slices recovered for at least another 30 minutes at room temperature prior to recording. For recording, slices were transferred to a recording chamber superfused with the same aCSF used in the recovery chamber, maintained at 32°C. Miniature excitatory postsynaptic currents (mEPSCs) were recorded in voltage-clamp mode (V_h = -76 mV) in the presence of 100 µM DL-AP5, 10 µM tetrodotoxin, and 20 µM gabazine (channel blockers acquired from Tocris). Glass pipettes pulled to a resistance of 2-6 MΩ were filled with internal solution containing the following (in mM): 130 K-gluconate, 10 KCl, 10 HEPES, 0.2 EGTA, 4 MgATP, 0.5 Na_2GTP, 10 Na_2-phosphocreatine, and 5 QX-314 chloride, pH adjusted to 7.3 with KOH, 280–290 mOsm. Pyramidal neurons in stratum pyramidale of CA1 in dorsal hippocampal slices were visually identified for recording. Only cells with a series resistance ≤ 30 MΩ, input resistance > 80 MΩ, and a resting membrane potential ≤ -50 mV were accepted for final analysis. Whole-cell parameters were monitored throughout the recording with a 100 ms, -10 mV step delivered every 30 sec. Recordings were made using an Axon MultiClamp 700B amplifier (Molecular Devices). Data were filtered at 2 kHz and digitized at 10 kHz with a National Instruments digital-analog converter under the control of Igor Pro software (WaveMetrics, RRID: SCR_000325). The frequency, amplitude, rise and decay times, and charge of mEPSCs were analyzed with Mini Analysis software (Synaptosoft, RRID: SCR_002184), with a threshold of 3× RMS noise for event discrimination. 100-200 well-isolated events were used for

these analyses in wild-type neurons; because of extremely low event frequency, a minimum of 50 events were used in knockout neurons.

Human induced pluripotent stem cell (iPSC)-derived cortical neural precursor cell cultures

iPSC lines were derived from peripheral blood obtained from eight individuals with autism and from four typically developing controls (DeRosa et al., 2018; Table 2). Peripheral blood mononuclear cells (PBMCs) were isolated and cultured in suspension until transduction using Oct4, Sox2, Klf4, and c-Myc Cytotune Sendai viruses (Life Technologies Cat# A16517) (DeRosa et al., 2012). After PBMC transduction into iPSCs the media was supplemented with 10 µM CHIR99021 (Stemgent Cat#04-0004-10), 1 µM PD325901 (Stemgent Cat#04-0006), 1 µM thiazovivin (Stemgent Cat#04-0017), and 10 µM Y27632 (Stemgent Cat#04-0012-10) for 7 days. At day 7, the media with small molecules was transitioned to mTeSR1 full stem cell maintenance media (Stemcell Technologies Cat#85850) with the media being changed daily. iPSC colonies were plated onto mouse embryonic feeders (MEFs) and grown for 7 days. Colonies were selected showing proliferating cell clusters, indicative of reprogrammed cells. To derive cortical progenitor neurons, selected iPSC colonies were dissociated via a 7-minute treatment with Accutase in the presence of 20 µM Y27632 and MEF feeders were removed using 0.1% gelatin as previously described (Nestor et al., 2015; Phillips, Nestor, & Nestor, 2017). Dissociated iPSCs were exposed to media containing small molecules (e.g. 10 µM Y27632, 10 µM SB431542 (Stemgent Cat#04-0010-10), 1 µM dorsomorphin (Stemgent Cat#04-0024), and 1 µM thiazovivin) within growth media as described previously (DeRosa et al., 2012). After patterning and neural induction, iPSC-derived neuron progenitors were expanded using 6-well plates coated with 15 µg/ml Poly-L-Ornithine (Millipore Sigma Cat# P4957) and 10 µg/ml laminin (Invitrogen Cat# 230171015) within an enriched medium containing 1:1 mixture of DMEM/F12 (with L-Glutamine; Thermo Fisher Cat# 11320-033) and Neurobasal medium (minus phenol red; Invitrogen Cat#12348017), 5 µM foreskolin (Millipore Sigma Cat# F6886), 60 ng/ml progesterone (Millipore Sigma Cat#P8783), 16 µg/ml putrescine (Millipore Sigma Cat#P7505), 5 µg/ml N-acetyl-L-cysteine (Millipore Sigma Cat#8199), 1% Insulin-Transferrin-Selenium-A (Gibco Cat#41400045), 1% B-27 supplement (Gibco Cat#12587010), 0.5% N2 supplement (Gibco Cat#17502048), 1% Antibiotic-Antimycotic, 30 ng/ml tri-iodothyronine (Millipore Sigma Cat#T6397), 40 ng/ml thyroxine (Millipore Sigma Cat#T1775), 0.5% non-essential amino acids, 100 µg/ml bovine-serum albumen (Millipore Sigma Cat#4161) and 0.5% GlutaMAX (Invitrogen Cat#35050061). Cells were harvested at 19 DIV in RIPA buffer (Cell Signaling Technologies Cat# 9806S) supplemented with PMSF (Cell Signaling Technologies Cat#8553S) and protease and phosphatase inhibitor cocktail (Thermo Fisher Scientific Cat#78442) and triplicates of each control and autism line were analyzed by Western blot.

Organoid culture and mRNA quantitation via qPCR

Cortical organoid cultures were generated from four control and six autism lines (Table 2) as previously described in Durens et al. (Durens et al., 2020). Organoids were cultured for 60 days, and then transferred to RNAprotect Cell Reagent (Qiagen Cat#76526) for RNA stabilization. Two organoids were pooled per biological replicate and triplicates of each control and autism line were analyzed. Samples were stored at -80°C until processed. Samples in RNAprotect were thawed on

ice and centrifuged at 5000 x g for 5 minutes after which supernatant was removed. Total RNA was extracted using the RiboPure Kit (Thermo Fisher Scientific Cat#AM1924) following manufacturer's specifications. RNA concentration was determined using NanoDrop 8000 Microvolume UV-Vis Spectrophotometer (Thermo Fisher Scientific). DNA-*free* DNA removal kit (Thermo Fisher Scientific Cat#AM1906) was used to remove residual DNA. Reverse transcription (RT) was performed using 250 ng of DNAse-treated RNA using the iScript cDNA synthesis kit (Bio-Rad Cat#1708890) and the resulting RT reactions were diluted 1:5 with nuclease-free water. qPCR was performed for the following genes: CDH8 (Forward – 5'-ACA GCG AAT TTT GAA CCG CTC-3'; Reverse – 5'- TCC TCC CGG TCA AGT CTT TTT -3') and CDH11 (Forward – 5'-AGA GGT CCA ATG TGG GAA CG -3', Reverse: 5'- GGT TGT CCT TCG AGG ATA CTG -3'). GAPDH was used as a reference gene (Genecopoeia Catalog#: HQP006940). qPCR was performed with 2X All-in-One qPCR Mix (Genecopoeia Catalog#: QP001) using the following reaction mix: 10µl All-in-One qPCR Mix (2x), 2 µl of 20µM primer, 5µl nuclease-free water, and 5 µl of cDNA at 1:5 dilution. Reactions were incubated at 95° for 10 minutes, followed by 40 cycles of 95° for 10 seconds, 60° for 20 seconds, and 72° for 30 seconds using the CFX96 Real-time System (Bio Rad). Melt curves were generated after amplification by increasing temperature from 72° to 95° at 0.5° increments. All reactions were performed in duplicates. Relative quantities for each gene were analyzed using the comparative Ct method. Fold changes were calculated relative to the average Ct values for control samples.

Statistical analysis

Statistical analysis was performed using Graph Pad Prism 8 software (GraphPad Prism Software, RRID: SCR_002798). Unpaired two-tailed *t*-test was performed when comparing two groups and one-way ANOVA with Tukey's or Dunnett's multiple comparison test was used to compare differences between three or four groups. *P*-values were considered significant if ≤ 0.05. Bar graphs are displayed as mean ± standard error of the mean (SEM).

Results

Cadherin-8 and cadherin-11 show similar temporal and spatial expression patterns

We compared the overall protein levels of classical type II cadherins cadherin-8 and cadherin-11 in C57BL/6 wild-type mouse whole brain samples taken at different ages of development from embryonic day (E) 14 to postnatal day (P) 21, as well as in adulthood by Western blot (Figure 1A). Cadherin-8 and cadherin-11 both exhibited relatively low expression at E14 but their levels increased postnatally. Cadherin-8 levels readily increased at P1 and reached more than a 10-fold increase by P7 and P14. The expression of Cadherin-8 dropped after P14 and remained at low levels in adulthood (Figure 1B). Cadherin-11 levels reached an approximately 2-fold increase by P7 and P14 compared to E14, but were reduced to P1 level by P21 and to E14 level by adulthood (Figure 1B). Comparison to the developmental timeline showed that cadherin-8 and cadherin-11 expression correlated to time points during which processes of dendrite development and synaptogenesis are prevalent, suggesting that they may play a roles in these processes. We then analyzed the protein levels in specific brain regions at P14 (Figure 1C, D). Cadherin-8 expression was significantly higher in the cortex, hippocampus and thalamus/striatum compared to the cerebellum. Cadherin-11 showed a similar expression pattern, although differences between regions were not statistically significant.

To further interrogate which brain cell type(s) express cadherins, protein levels of cadherin-8 and cadherin-11 were measured in primary cortical neurons and glial cells cultured from mouse cortices. The temporal expression patterns of cadherin-8 and cadherin-11 in primary cortical neurons showed a gradual increase of both cadherins from 1 DIV to 14 DIV, recapitulating the temporal expression profile observed in the mouse whole brain tissue (Supplementary Figure 3A, B). In contrast to neurons, cadherin-8 was virtually undetectable in primary glial cells (Supplementary Figure 3C). Cadherin-11 was expressed in both cortical neurons and glial cells, but the protein levels in neurons were two-fold greater than in glial cells (Supplementary Figure 3D). These results demonstrate that both cadherins are preferentially expressed in neurons.

Cadherin-8 is preferentially expressed in excitatory neurons and binds to neuroligin-1

We next performed subcellular fractionation of forebrain tissue to isolate synaptic plasma membrane (SPM) and postsynaptic density (PSD) to determine whether cadherins are enriched in synaptic compartments (Figure 2A, B). The distribution of PSD-95, syntaxin-1, and β-actin were evaluated to confirm successful separation and purity of different subcellular fractions. PSD-95 was used as a positive control for protein enrichment in SPM and PSD fractions - it was significantly enriched in SPM and PSD fractions compared to total protein input (Figure 2B). Syntaxin-1 was enriched in synaptosome (P3), SPM, and synaptic vesicles (S3), consistent with its localization in the presynaptic membrane and its function in vesicle release. Cadherin-8 was enriched 3.7-fold in the PSD fraction and cadherin-11 was enriched 2.6- and 3.4-fold in the SPM and PSD fractions, respectively, compared to unfractionated lysate (Figure 2B).

Since cadherin-8 and cadherin-11 expression were both enriched in the PSD, we performed co-immunoprecipitation (co-IP) experiments using anti-Cdh8 (Figure 2C) and anti-Cdh11 antibodies (Figure 2D) to determine the association of these two cadherins with specific postsynaptic proteins. Both cadherin-8 and cadherin-11 immunoprecipitated β-catenin, the

conserved intracellular binding partner of classical cadherins (Seong et al., 2015). Neither cadherin-8 nor cadherin-11 co-immunoprecipitated with PSD-95 or N-cadherin. Previous studies found cooperative functions of classical cadherins with the excitatory synaptic adhesion molecule neuroligin-1 (Nlgn1) during neural circuit development (Aiga, Levinson, & Bamji, 2011; Stan et al., 2010; Yamagata, Duan, & Sanes, 2018). This prompted us to investigate whether cadherin-8 and cadherin-11 physically interact with neuroligin-1. Interestingly, neuroligin-1 was detected in the immunoprecipitate of cadherin-8, but not cadherin-11. We confirmed this interaction *in vitro* by co-expressing myc-tagged *Cdh8* together with HA-tagged *Nlgn1* in N2a cells that do not express either protein (Supplementary Figure 4). Using either anti-HA or anti-myc antibodies to selectively pull down neuroligin-1 and cadherin-8, respectively, we found that neuroligin-1 co-immunoprecipitated cadherin-8 and vice versa. Consistent with these findings, immunostaining of N2a cells overexpressing myc-tagged *Cdh8* and HA-tagged *Nlgn1* showed a partial co-localization of these two proteins at the plasma membrane and at cell-cell contacts (Figure 2E).

The finding of an interaction of cadherin-8 with neuroligin-1 prompted us to further examine the subcellular localization of cadherin-8 in neurons. The specificity of the anti-cadherin-8 antibody was first validated in immunocytochemistry (Supplementary Figure 1C). Immunofluorescence of surface-exposed cadherin-8 in 15 DIV hippocampal neurons revealed partial co-localization with the excitatory synaptic markers PSD-95 and synapsin-1 (Figure 3A). The majority of cadherin-8 localized to excitatory synaptic puncta, either co-localizing with PSD-95 (30.3% ± 2.0%) or located directly adjacent to PSD-95-positive puncta (41.6% ± 2.5%), while the remainder of cadherin-8 puncta (28.1% ± 2.2%) did not localize to PSD-95-positive puncta (Figure 3C). Hence, most, but not all, cadherin-8-positive puncta are associated with synapses. Conversely, the majority of the cadherin-8-positive puncta did not associate with GAT-1-positive puncta, markers of inhibitory synapses (56.8% ± 3.4%; Figure 3B and D). However, a small fraction of cadherin-8-positive puncta exhibited co-localization with (10.0% ± 1.8%) or were adjacent to GAT-1-positive puncta (33.2% ± 2.6%). These data suggest that cadherin-8 is enriched at/near excitatory synapses compared to inhibitory synapses, consistent with the potential role in excitatory synaptic function. We performed direct stochastic reconstruction microscopy (dSTORM) to further quantify cadherin-8 presence at excitatory synapses. We examined the distance between PSD-95 and either cadherin-8 or neuroligin-1, a positive control for excitatory synaptic localization (Figure 3E, F). For optimal two-color imaging, we used an Oxyfluor buffer system (Nahidiazar et al., 2016). 33.3% ± 3.3% of cadherin-8 puncta were located within 50 nm of a PSD-95 puncta, significantly more than a randomized set of data points (13.7% ± 1.0%; Figure 3G, I, J). This recapitulates the co-localization data obtained using standard confocal microscopy. Interestingly, dSTORM imaging showed that significantly more neuroligin-1 puncta were within 50 nm of a PSD-95 punctum (52% ± 3.8%) compared to cadherin-8 puncta and the randomized data points (Figure 3H, I, J). Together, these data indicate that cadherin-8 localizes to excitatory synapses but to a lesser extent than neuroligin-1. These findings are in line with the localization of cadherin-8 and neuroligin-1 in N2a cells suggesting that these two proteins partially but not completely localize to the same cellular compartment.

Elevated cadherin-8 expression in *Cdh11*$^{-/-}$ mice is accompanied by an increase of excitatory synaptic proteins and dendrite complexity

Our results suggest that cadherin-8 and cadherin-11 share partially overlapping expression patterns. Alterations in excitatory synapse development is one of the hallmarks of autism (Forrest, Parnell, & Penzes, 2018; Hutsler & Zhang, 2010). The *Cdh11* knockout mouse provided a means to further examine the relationship between cadherin-8 and cadherin-11 and their potential contributions to excitatory synaptic development (Horikawa et al., 1999). Western blot analysis from P7 whole brain tissue confirmed that cadherin-11 was not detected in *Cdh11*$^{-/-}$ brains (Figure 4A, B), while levels of cadherin-8 were significantly increased in *Cdh11*$^{-/-}$ brains (Figure 4A, C). This result indicates that cadherin-8 may exert a compensatory function in the absence of cadherin-11.

Since we identified neuroligin-1 as a selective binding partner of cadherin-8, and neuroligin-1 has been shown to be selectively involved in the development of excitatory synapses (Song, Ichtchenko, Südhof, & Brose, 1999), we reasoned that neuroligin-1 levels may be altered in *Cdh11*$^{-/-}$ brains. Indeed, Western blot analysis from P7 *Cdh11*$^{-/-}$ whole brain lysates showed that neuroligin-1 was significantly increased compared to wild-type littermates (Figure 4D, E). PSD-95 expression was also significantly increased in *Cdh11*$^{-/-}$ brains (Figure 4D, F). In contrast, there was no difference in levels of the inhibitory synaptic marker gephyrin (Figure 4D, G). We then examined the density of dendritic spines, the major structures that harbor excitatory synapses, in 15 DIV hippocampal cultures from *Cdh11* wild-type and knockout mice (Figure 4H). Intriguingly, we did not observe changes in the dendritic spine density on primary, secondary and tertiary dendrites of *Cdh11*$^{-/-}$ neurons compared to wild-type neurons (Figure 4I; Primary – WT: 0.7664 ± 0.0301 μm^{-1}, KO: 0.7086 ± 0.0428 μm^{-1}; Secondary – WT: 0.7070 ± 0.0270 μm^{-1}, KO: 0.6527 ± 0.0301 μm^{-1}; Tertiary – WT: 0.6051 ± 0.0265 μm^{-1}, KO: 0.6440 ± 0.0337 μm^{-1}; Total – WT: 0.6778 ± 0.0194 μm^{-1}, KO: 0.6607 ± 0.0299 μm^{-1}). We next analyzed the dendritic morphology of *Cdh11* knockout and wild-type neurons from 15 DIV hippocampal cultures. Sholl analysis revealed an increase in the dendritic arbor complexity in *Cdh11*$^{-/-}$ neurons (area under the curve (AUC): 3,051 ± 156) compared to wild-type neurons (Figure 4J, K; AUC: 2,551 ± 153.1). The increase in dendritic complexity resulted from a significant increase in total dendrite length (Figure 4L; WT: 2,509 ± 174 μm, KO: 3,034 ± 162.7 μm) as well as branches as revealed by branch tip number (Figure 4M; WT: 29.17 ± 2.194, KO: 35.4 ± 1.48). These data suggest that the overall increased dendritic complexity of *Cdh11* knockout neurons may result in an increase of excitatory postsynaptic sites without changing the spine density.

Cdh11$^{-/-}$ mice exhibit altered calcium activity and miniature excitatory postsynaptic currents

The increase in excitatory synaptic protein expression in *Cdh11*$^{-/-}$ brains and the increased dendritic arborization in *Cdh11*$^{-/-}$ neurons prompted us to investigate whether deletion of *Cdh11* results in changes in neuronal and synaptic activity. We first transduced hippocampal neurons prepared from *Cdh11* knockout and wild-type mice with the NeuroBurst Orange lentivirus (EssenBioscience Sartorius) and imaged network calcium activity using the IncuCyte S3 Live-Cell Analysis System for Neuroscience (EssenBioscience Sartorius) at 15 DIV (Figure 5A) for 24 hours. Interestingly, *Cdh11* knockout cultures showed significantly fewer active neurons compared to wild-type cultures (Figure 5B; WT: 1,756 ± 109.9, KO: 1,238 ± 159.1), although there was no difference in total cell number or infection rate between genotypes (Supplementary

Figure 5). In addition, the activity of *Cdh11*$^{-/-}$ neurons was significantly less correlated when compared to wild-type neurons (Figure 5C; WT: 1.405 ± 0.0681, KO: 1.111 ± 0.0657). *Cdh11*$^{-/-}$ neurons further exhibited significantly reduced mean burst strengths (Figure 5D; WT: 0.6473 ± 0.0507, KO: 0.4163 ± 0.0324), whereas mean burst rate was similar in *Cdh11* knockout and wild-type cultures (Figure 5E; WT: 3.643 ± 0.9519 min^{-1}, KO: 4.983 ± 1.424 min^{-1}). Together, these data show that *Cdh11* knockout neurons exhibit a significant reduction in neuronal activity compared to wild-type neurons.

Because of the altered dendritic morphology and changes in calcium activity in *Cdh11* knockout cultures, we next asked whether deletion of cadherin-11 affects the function of hippocampal synapses in the whole organism. We used *ex vivo* hippocampal slices to examine the effects of *Cdh11* knockout on AMPAR-mediated miniature excitatory postsynaptic currents (mEPSCs) in CA1 pyramidal cells from wild-type and knockout mice aged P21-P24 (Figure 5F, G). We found that miniature EPSC frequency was significantly lower in CA1 pyramidal cells from *Cdh11* knockout mice compared to wild-type littermates (Figure 5H; WT: 1.16 ± 0.1254 Hz, KO: 0.5026 ± 0.0445 Hz). Conversely, mEPSC amplitude was higher in *Cdh11* knockout neurons (Figure 5I; WT: 11.28 ± 0.4684 pA, KO: 14.12 ± 1.078 pA). Analysis of the kinetics of CA1 mEPSCs found that there was no difference in the charge (Figure 5J; WT: 76.92 ± 4.035 fC, KO: 91.56 ± 6.325 fC), rise time (Figure 5K; WT: 1.355 ± 0.044 ms, KO: 1.355 ± 0.064 ms) or decay time constant between *Cdh11* knockout and wild-type mice (Figure 5L; WT: 4.940 ± 0.194 ms, KO: 5.091 ± 0.228 ms). These data, demonstrating a reduction of mEPSC frequency and a concurrent increase in mEPSC amplitude in *Cdh11* knockout hippocampus, supports the important role of cadherin-11 in the formation and maintenance of synaptic networks. Combined with our earlier data from cultured hippocampal neurons, the data suggest that loss of cadherin-11 results in disturbed synaptic transmission potentially by reduced functional synaptic input to postsynaptic cells.

CDH8 and CDH11 levels are altered in autism-specific iPSC-derived cortical neuronal progenitor cells and organoids

As autism spectrum disorder is a genetically complex condition with broad heterogeneity across individuals, we investigated the expression of CDH8 and CDH11 in human tissue using samples from autistic and typically-developing control individuals to determine whether the levels of these cadherins are commonly altered in autism. iPSC-derived cortical neural progenitor cells (NPCs) from four neurotypical control and eight autistic individuals were cultured for 19 DIV and cell lysates were harvested for protein analysis (Table 2; Figure 6A, B). Although none of these individuals carried risk variants in either of these cadherins (DeRosa et al., 2018), CDH8 levels were significantly increased (Figure 6A) whereas CDH11 levels were significantly decreased (Figure 6B) in iPSC-derived cortical NPCs from autistic individuals compared to neurotypical control cells. This expression pattern recapitulated the expression profile observed in the *Cdh11* knockout mice and supported the use of this mouse to investigate potential mechanistic alterations occurring in autism. We next performed quantitative PCR (qPCR) to analyze mRNA expression of CDH8 and CDH11 in iPSC-derived cortical organoids generated from autistic and typically-developing control individuals that were grown in culture for 60 DIV (Table 2; Figure 6C, D). These cortical organoids mimic early cortical development with active excitatory and inhibitory neurotransmission (Durens et al., 2020). In line with the expression profile in the NPCs, autism-

specific iPSC-derived cortical organoids showed a significant increase of CDH8 (Figure 6C) and a concomitant decrease of CDH11 (Figure 6D) compared to neurotypical control organoids. Together, these results show that cadherin expression levels are altered in cells derived from individuals with autism during early stages of neural circuit development. The differences in expression between the autism-specific iPSC-derived neurons and neurotypical control neurons suggest a potential role of CDH8 and CDH11 in autism pathophysiology.

Discussion

In this study, we used mouse tissues to systematically investigate the expression, localization and function of the autism candidate risk genes cadherin-8 and cadherin-11. The comprehensive expression analysis revealed that both of these type II classical cadherins are expressed in the developing mouse brain at the right time and right place to regulate crucial steps in neural circuit formation and to impact normal brain development. The analysis of *Cdh11*$^{-/-}$ mouse brains further suggests putative mechanisms to explain cellular and circuitry phenotypes observed in autism. Expression analysis of cadherin-8 and cadherin-11 in NPCs and mature organoids generated from autistic individuals demonstrate that levels of these two cadherins are altered throughout early neural circuit development in autism. Together, our study not only reveals a detailed and novel characterization of the autism-risk cadherins cadherin-8 and cadherin-11, but also provides insights into the potential contributions of these cadherins in neural circuit formation and the neurodevelopment of autism.

The cadherin superfamily consists of numerous subfamily members with similar protein structures but distinct functions. Both, cadherin-8 and cadherin-11 belong to the same classical type II cadherin subfamily. In addition to a similar structure, several studies have found similar expression profiles and functions of cadherin-8 and cadherin-11 in the brain. Cadherin-8 is important for synaptic targeting in the hippocampus (Bekirov, Nagy, Svoronos, Huntley, & Benson, 2008), striatum (Friedman, Riemslagh, et al., 2015), and visual system (Duan, Krishnaswamy, De la Huerta, & Sanes, 2014; Osterhout et al., 2011). Cadherin-11 is also strongly expressed in the hippocampus and functions at glutamatergic synapses (Bartelt-Kirbach, Langer-Fischer, & Golenhofen, 2010; Manabe et al., 2000; Paradis et al., 2007). In agreement with these studies, our spatial expression analysis showed that cadherin-8 and cadherin-11 are enriched in similar brain regions including cortex, hippocampus, and thalamus/striatum. The temporal expression analysis showed that both cadherins exhibit peak expression in postnatal brains at the time window that coincides with dendrite development and synaptogenesis, processes that have been adversely implicated in the developing autism brain (Betancur et al., 2009; Bourgeron, 2009; Hussman et al., 2011). In particular, cadherin-8 exhibited a dramatic but transient increase from embryonic stage to the first postnatal week. Protein levels quickly declined later in development and remained low in adulthood. This surge in expression strongly indicates a specific role for cadherin-8 in regulating dendrite and synapse development. In contrast, cadherin-11 expression levels were relatively steady before and after the peak increase at an early postnatal age. This overlooked difference between cadherin-8 and cadherin-11 may indicate at least partially divergent signaling pathways and functions mediated by these two closely related cadherins.

In addition, we found neuroligin-1 as a selective interaction partner of cadherin-8, but not of cadherin-11. Although cadherin-8 levels were consistently increased in the absence of cadherin-11, potentially due to compensation, the selective interaction between cadherin-8 and neuroligin-1 may explain why the loss of cadherin-11 results in altered cellular and physiological phenotypes. Morphometric analysis of *Cdh11* knockout neurons revealed an increased complexity of dendritic arbors. This may be due to the increase of cadherin-8, as knockdown of cadherin-8 in rat cortical neurons has been shown to impair dendritic arborization (Friedman, Riemslagh, et al., 2015). Subsequently, the increase of dendrites may provide more available potential synaptic contacts even though the density of dendritic spines is not changed. The increases of PSD-95 and neuroligin-1 reflect an increase in potential excitatory postsynaptic sites, where cadherin-8 may also regulate synaptic function by interacting with neuroligin-1.

The increase of excitatory postsynaptic sites coupled with a reduction in calcium activity, as indicated by the decreased correlation of activity and fewer active cells, as well as the reduction in mEPSC frequency in *Cdh11* knockout mice suggests disruption of functional synaptic input onto postsynaptic neurons. As a compensatory mechanism, neurons may increase postsynaptic strength, as shown by the higher mEPSC amplitude, and search for more synaptic input, as shown by the increased dendritic arborization and the increase in postsynaptic markers, in an effort to reach homeostatic levels of input and activity. In line with this interpretation, calcium-imaging further showed that *Cdh11* knockout neurons exhibited significantly reduced mean burst strengths, reflecting an overall decrease in somatic calcium influx and potentially reduced neuronal activity. Interestingly, *Cdh11* and *Nlgn1* knockout mice both exhibit behavioral deficits similar to phenotypes observed in autism (Blundell et al., 2010; Wu et al., 2020), although *Nlgn1* knockout animals exhibit impairment of excitatory synaptic function (Chanda, Hale, Zhang, Wernig, & Südhof, 2017; Chubykin et al., 2007). This suggests that alterations in the number of excitatory synapses in any direction is expected to disrupt the balance of excitation and inhibition in neuronal circuitry, a common phenotype that has been observed in autism (Blatt et al., 2001; Gao & Penzes, 2015; Hussman, 2001). Further investigations are required to help elucidate a potential mechanism underlying the altered synaptic activity in *Cdh11* knockout brains.

Members of the cadherin superfamily have emerged as candidate risk genes for autism in multiple independent association studies (Camacho et al., 2012; Chapman et al., 2011; Crepel et al., 2014; Cukier et al., 2014; Depienne et al., 2009; Girirajan et al., 2013; Hussman et al., 2011; Kenny et al., 2014; Marshall et al., 2008; Morrow et al., 2008; Neale et al., 2012; O'Roak et al., 2012; Pagnamenta et al., 2011; Sanders et al., 2011; van Harssel et al., 2013; K. Wang et al., 2009; Willemsen et al., 2010). Despite these findings, no autism case reported to date has resulted from monogenic alterations in cadherins. In fact, none of the individuals with autism tested in this study harbor damaging mutations in the *CDH8* or *CDH11* genes (DeRosa et al., 2018). Yet, these individuals consistently show altered expression patterns in CDH8 and CDH11 throughout neural development from neural precursor cells to more mature organoids. This suggests that a pathway involving CDH8 and CDH11 may be vulnerable in autism and that the balance of these two cadherins may be important for normal brain function. In addition to specific autism-associated mutations in cadherins, these molecules may be part of a broader pathway involving other genes mutated in autism. Indeed, some of the autism lines examined in this study were also reported to display misregulation of genes involved in cell-cell signaling and actin cytoskeleton signaling, both processes that involve cadherins (DeRosa et al., 2018). The overall decrease in synaptic activity that we observed in the *Cdh11* knockout neurons is consistent with the phenotypic characterization of the iPSC-derived cortical neurons from autistic individuals performed by DeRosa et. al., as they reported decreased spontaneous spiking activity, as well as decreased number of calcium transients in these neurons. The autism-specific iPSC-derived cortical neurons also exhibited decreased migration of neuronal processes (DeRosa et al., 2018). Interestingly, elevated expression of CDH11 has been observed in glioblastoma and has been associated with increased cell migration (Schulte et al., 2013). Thus, the reduced migration ability of the autism-specific neurons may stem from the decreased CDH11 expression that we observed in these autism lines. These findings further emphasize the significance of our effort to investigate the involvement of CDH8 and CDH11 in autism.

To our knowledge, our study is the first to show that cadherin levels are altered in cells derived from individuals with autism. Based on the known functions of cadherins, both lower and

higher expression levels could directly affect neuronal connectivity by altering cell-cell adhesion, downstream signaling and consequently synaptic function. The findings of this study strengthen the hypothesis that cadherin signaling may represent an important pathway affected in autism. Our current study suggests that excitatory neuronal development is a common function mediated by cadherin-8 and cadherin-11. However, upstream factors affecting the expression of cadherin-8 and cadherin-11 still require further investigation. Future studies should also aim to identify mechanisms that connect different cadherins to other synaptic cell adhesion molecules. Such a potential connection is described here between cadherin-8 and neuroligin-1, another autism risk candidate adhesion molecule (Nakanishi et al., 2017). In conclusion, our study shows that cadherin-8 and cadherin-11 play an important role in regulating excitatory neuronal development, and that altered expression of these two cadherins likely contributes in part to the etiology of autism.

Funding

This work is supported by Hussman Foundation grants HIAS#15007 and HIAS#18005 to JAF, HIAS#18001 to SH, and HIAS#15003 and HIAS#18004 to YCL.

Conflict of Interest

The authors declare that the research was conducted in the absence of any commercial or financial relationships that could be construed as a potential conflict of interest.

Acknowledgements

We want to thank Dr. Celine Plachez at the Hussman Institute for Autism for the technical support. We also want to thank Drs. Louis DeTolla and Turhan Coksaygan at the University of Maryland School of Medicine for providing veterinary services and consultation. We thank Dr. Olga Latinovic from the imaging core at the Institute of Human Virology at the University of Maryland School of Medicine for her help and assistance with the dSTORM imaging. Finally, we thank Drs. John Hussman, Thomas Blanpied, and Anthony Koleske for the critical evaluation of this manuscript.

Author contribution statement

JF, YL: Conceptualization. JF, RN, MB, MD, JN, XY, MN, SH, YL: Methodology. JF, RN, MB, MD, YL: Investigation. JF, RN, MB, MD, YL: Formal Analysis. JF, YL: Writing – Original draft. JF, RN, MB, MD, JN, XY, DD, MN, SH, GB, YL: Writing – Review and Editing. JF, YL: Visualization. DD, MN, SH, GB, YL: Supervision. JF, YL: Project Administration. JF, SH, YL: Funding Acquisition.

Contribution to the field

Autism is a neurodevelopmental condition with high genetic and phenotypic heterogeneity. Multiple genes have been implicated in autism. Among them, the cadherin superfamily of adhesion molecules represent significant numbers of candidates. This study implicates roles of the classical type II cadherins, cadherin-8 and cadherin-11, in the development of neural circuits and provides novel insights into the association of these two cell adhesion molecules with autism. First, the temporal and spatial expression pattern suggests that these two cadherins might act as regulators of crucial steps during normal development of the nervous system, such as dendrite development and synaptogenesis. Second, loss of cadherin-11 changes the expression level of not only cadherin-8 and other proteins associated with excitatory synapses but also alters the morphology and activity of excitatory neurons. Third, altered expression of cadherin-8 and cadherin-11 in human tissue samples of autistic individuals suggests a direct effect of these molecules on neuronal function in humans. Taken together, this study reveals novel contributions of two classical type II cadherins in neural circuit formation and strengthens the hypothesis that they may contribute to aspects of autism pathophysiology.

Data availability statement

The dataset supporting the conclusions of this study are available upon reasonable request by the corresponding authors.

693 **References**

694 American Psychiatric Association (2013). Diagnostic and Statistical Manual of Mental Disorders,
695 5th Edn. Arlington, VA: American Psychiatric Publishing
696 Aiga, M., Levinson, J. N., & Bamji, S. X. (2011). N-cadherin and neuroligins cooperate to
697 regulate synapse formation in hippocampal cultures. *J Biol Chem, 286*(1), 851-858.
698 doi:10.1074/jbc.M110.176305
699 Arikkath, J., & Reichardt, L. F. (2008). Cadherins and catenins at synapses: roles in
700 synaptogenesis and synaptic plasticity. *Trends Neurosci, 31*(9), 487-494.
701 doi:10.1016/j.tins.2008.07.001
702 Baio, J., Wiggins, L., Christensen, D. L., Maenner, M. J., Daniels, J., Warren, Z., . . . Dowling,
703 N. F. (2018). Prevalence of Autism Spectrum Disorder Among Children Aged 8 Years -
704 Autism and Developmental Disabilities Monitoring Network, 11 Sites, United States,
705 2014. *MMWR Surveill Summ, 67*(6), 1-23. doi:10.15585/mmwr.ss6706a1
706 Bartelt-Kirbach, B., Langer-Fischer, K., & Golenhofen, N. (2010). Different regulation of N-
707 cadherin and cadherin-11 in rat hippocampus. *Cell Commun Adhes, 17*(4-6), 75-82.
708 doi:10.3109/15419061.2010.549977
709 Basu, R., Taylor, M. R., & Williams, M. E. (2015). The classic cadherins in synaptic specificity.
710 *Cell Adh Migr, 9*(3), 193-201. doi:10.1080/19336918.2014.1000072
711 Bekirov, I. H., Nagy, V., Svoronos, A., Huntley, G. W., & Benson, D. L. (2008). Cadherin-8 and
712 N-cadherin differentially regulate pre- and postsynaptic development of the hippocampal
713 mossy fiber pathway. *Hippocampus, 18*(4), 349-363. doi:10.1002/hipo.20395
714 Bermejo, M. K., Milenkovic, M., Salahpour, A., & Ramsey, A. J. (2014). Preparation of synaptic
715 plasma membrane and postsynaptic density proteins using a discontinuous sucrose
716 gradient. *J Vis Exp*(91), e51896. doi:10.3791/51896
717 Betancur, C., Sakurai, T., & Buxbaum, J. D. (2009). The emerging role of synaptic cell-adhesion
718 pathways in the pathogenesis of autism spectrum disorders. *Trends Neurosci, 32*(7), 402-
719 412. doi:10.1016/j.tins.2009.04.003
720 Blatt, G. J., Fitzgerald, C. M., Guptill, J. T., Booker, A. B., Kemper, T. L., & Bauman, M. L.
721 (2001). Density and distribution of hippocampal neurotransmitter receptors in autism: an
722 autoradiographic study. *J Autism Dev Disord, 31*(6), 537-543.
723 Blundell, J., Blaiss, C. A., Etherton, M. R., Espinosa, F., Tabuchi, K., Walz, C., . . . Powell, C.
724 M. (2010). Neuroligin-1 deletion results in impaired spatial memory and increased
725 repetitive behavior. *J Neurosci, 30*(6), 2115-2129. doi:10.1523/JNEUROSCI.4517-
726 09.2010
727 Bourgeron, T. (2009). A synaptic trek to autism. *Curr Opin Neurobiol, 19*(2), 231-234.
728 doi:10.1016/j.conb.2009.06.003
729 Bourgeron, T. (2015). From the genetic architecture to synaptic plasticity in autism spectrum
730 disorder. *Nat Rev Neurosci, 16*(9), 551-563. doi:10.1038/nrn3992
731 Camacho, A., Simón, R., Sanz, R., Viñuela, A., Martínez-Salio, A., & Mateos, F. (2012).
732 Cognitive and behavioral profile in females with epilepsy with PDCH19 mutation: two
733 novel mutations and review of the literature. *Epilepsy Behav, 24*(1), 134-137.
734 doi:10.1016/j.yebeh.2012.02.023
735 Chanda, S., Hale, W. D., Zhang, B., Wernig, M., & Südhof, T. C. (2017). Unique versus
736 Redundant Functions of Neuroligin Genes in Shaping Excitatory and Inhibitory Synapse
737 Properties. *J Neurosci, 37*(29), 6816-6836. doi:10.1523/JNEUROSCI.0125-17.2017

738 Chapman, N. H., Estes, A., Munson, J., Bernier, R., Webb, S. J., Rothstein, J. H., . . . Wijsman,
739 E. M. (2011). Genome-scan for IQ discrepancy in autism: evidence for loci on
740 chromosomes 10 and 16. *Hum Genet, 129*(1), 59-70. doi:10.1007/s00439-010-0899-z
741 Chen, J., Yu, S., Fu, Y., & Li, X. (2014). Synaptic proteins and receptors defects in autism
742 spectrum disorders. *Front Cell Neurosci, 8*, 276. doi:10.3389/fncel.2014.00276
743 Chih, B., Gollan, L., & Scheiffele, P. (2006). Alternative splicing controls selective trans-
744 synaptic interactions of the neuroligin-neurexin complex. *Neuron, 51*(2), 171-178.
745 doi:10.1016/j.neuron.2006.06.005
746 Chubykin, A. A., Atasoy, D., Etherton, M. R., Brose, N., Kavalali, E. T., Gibson, J. R., &
747 Südhof, T. C. (2007). Activity-dependent validation of excitatory versus inhibitory
748 synapses by neuroligin-1 versus neuroligin-2. *Neuron, 54*(6), 919-931.
749 doi:10.1016/j.neuron.2007.05.029
750 Crepel, A., De Wolf, V., Brison, N., Ceulemans, B., Walleghem, D., Peuteman, G., . . . Peeters,
751 H. (2014). Association of CDH11 with non-syndromic ASD. *Am J Med Genet B*
752 *Neuropsychiatr Genet, 165B*(5), 391-398. doi:10.1002/ajmg.b.32243
753 Cukier, H. N., Dueker, N. D., Slifer, S. H., Lee, J. M., Whitehead, P. L., Lalanne, E., . . . Pericak-
754 Vance, M. A. (2014). Exome sequencing of extended families with autism reveals genes
755 shared across neurodevelopmental and neuropsychiatric disorders. *Mol Autism, 5*(1), 1.
756 doi:10.1186/2040-2392-5-1
757 Depienne, C., Bouteiller, D., Keren, B., Cheuret, E., Poirier, K., Trouillard, O., . . . Leguern, E.
758 (2009). Sporadic infantile epileptic encephalopathy caused by mutations in PCDH19
759 resembles Dravet syndrome but mainly affects females. *PLoS Genet, 5*(2), e1000381.
760 doi:10.1371/journal.pgen.1000381
761 DeRosa, B. A., El Hokayem, J., Artimovich, E., Garcia-Serje, C., Phillips, A. W., Van Booven,
762 D., . . . Dykxhoorn, D. M. (2018). Convergent Pathways in Idiopathic Autism Revealed
763 by Time Course Transcriptomic Analysis of Patient-Derived Neurons. *Sci Rep, 8*(1),
764 8423. doi:10.1038/s41598-018-26495-1
765 DeRosa, B. A., Van Baaren, J. M., Dubey, G. K., Lee, J. M., Cuccaro, M. L., Vance, J. M., . . .
766 Dykxhoorn, D. M. (2012). Derivation of autism spectrum disorder-specific induced
767 pluripotent stem cells from peripheral blood mononuclear cells. *Neurosci Lett, 516*(1), 9-
768 14. doi:10.1016/j.neulet.2012.02.086
769 Duan, X., Krishnaswamy, A., De la Huerta, I., & Sanes, J. R. (2014). Type II cadherins guide
770 assembly of a direction-selective retinal circuit. *Cell, 158*(4), 793-807.
771 doi:10.1016/j.cell.2014.06.047
772 Durens, M., Nestor, J., Williams, M., Herold, K., Niescier, R. F., Lunden, J. W., . . . Nestor, M.
773 W. (2020). High-throughput screening of human induced pluripotent stem cell-derived
774 brain organoids. *J Neurosci Methods, 335*, 108627. doi:10.1016/j.jneumeth.2020.108627
775 Ferreira, T. A., Blackman, A. V., Oyrer, J., Jayabal, S., Chung, A. J., Watt, A. J., . . . van Meyel,
776 D. J. (2014). Neuronal morphometry directly from bitmap images. *Nat Methods, 11*(10),
777 982-984. doi:10.1038/nmeth.3125
778 Forrest, M. P., Parnell, E., & Penzes, P. (2018). Dendritic structural plasticity and
779 neuropsychiatric disease. *Nat Rev Neurosci, 19*(4), 215-234. doi:10.1038/nrn.2018.16
780 Friedman, L. G., Benson, D. L., & Huntley, G. W. (2015). Cadherin-based transsynaptic
781 networks in establishing and modifying neural connectivity. *Curr Top Dev Biol, 112*,
782 415-465. doi:10.1016/bs.ctdb.2014.11.025

783 Friedman, L. G., Riemslagh, F. W., Sullivan, J. M., Mesias, R., Williams, F. M., Huntley, G. W.,
784 & Benson, D. L. (2015). Cadherin-8 expression, synaptic localization, and molecular
785 control of neuronal form in prefrontal corticostriatal circuits. *J Comp Neurol, 523*(1), 75-
786 92. doi:10.1002/cne.23666
787 Gao, R., & Penzes, P. (2015). Common mechanisms of excitatory and inhibitory imbalance in
788 schizophrenia and autism spectrum disorders. *Curr Mol Med, 15*(2), 146-167.
789 Girirajan, S., Dennis, M. Y., Baker, C., Malig, M., Coe, B. P., Campbell, C. D., . . . Eichler, E. E.
790 (2013). Refinement and discovery of new hotspots of copy-number variation associated
791 with autism spectrum disorder. *Am J Hum Genet, 92*(2), 221-237.
792 doi:10.1016/j.ajhg.2012.12.016
793 Gu, Y., & Huganir, R. L. (2016). Identification of the SNARE complex mediating the exocytosis
794 of NMDA receptors. *Proc Natl Acad Sci U S A, 113*(43), 12280-12285.
795 doi:10.1073/pnas.1614042113
796 Hirano, S., & Takeichi, M. (2012). Cadherins in brain morphogenesis and wiring. *Physiol Rev,*
797 *92*(2), 597-634. doi:10.1152/physrev.00014.2011
798 Horikawa, K., Radice, G., Takeichi, M., & Chisaka, O. (1999). Adhesive subdivisions intrinsic
799 to the epithelial somites. *Dev Biol, 215*(2), 182-189. doi:10.1006/dbio.1999.9463
800 Huguet, G., Ey, E., & Bourgeron, T. (2013). The genetic landscapes of autism spectrum
801 disorders. *Annu Rev Genomics Hum Genet, 14*, 191-213. doi:10.1146/annurev-genom-
802 091212-153431
803 Hulpiau, P., & van Roy, F. (2009). Molecular evolution of the cadherin superfamily. *Int J*
804 *Biochem Cell Biol, 41*(2), 349-369. doi:10.1016/j.biocel.2008.09.027
805 Hussman, J. P. (2001). Suppressed GABAergic inhibition as a common factor in suspected
806 etiologies of autism. *J Autism Dev Disord, 31*(2), 247-248.
807 Hussman, J. P., Chung, R. H., Griswold, A. J., Jaworski, J. M., Salyakina, D., Ma, D., . . .
808 Pericak-Vance, M. A. (2011). A noise-reduction GWAS analysis implicates altered
809 regulation of neurite outgrowth and guidance in autism. *Mol Autism, 2*(1), 1.
810 doi:10.1186/2040-2392-2-1
811 Hutsler, J. J., & Zhang, H. (2010). Increased dendritic spine densities on cortical projection
812 neurons in autism spectrum disorders. *Brain Res, 1309*, 83-94.
813 doi:10.1016/j.brainres.2009.09.120
814 Inoue, T., Tanaka, T., Suzuki, S. C., & Takeichi, M. (1998). Cadherin-6 in the developing mouse
815 brain: expression along restricted connection systems and synaptic localization suggest a
816 potential role in neuronal circuitry. *Dev Dyn, 211*(4), 338-351. doi:10.1002/(SICI)1097-
817 0177(199804)211:4<338::AID-AJA5>3.0.CO;2-I
818 Jeste, S. S., & Geschwind, D. H. (2014). Disentangling the heterogeneity of autism spectrum
819 disorder through genetic findings. *Nat Rev Neurol, 10*(2), 74-81.
820 doi:10.1038/nrneurol.2013.278
821 Joensuu, M., Lanoue, V., & Hotulainen, P. (2017). Dendritic spine actin cytoskeleton in autism
822 spectrum disorder. *Prog Neuropsychopharmacol Biol Psychiatry*.
823 doi:10.1016/j.pnpbp.2017.08.023
824 Kenny, E. M., Cormican, P., Furlong, S., Heron, E., Kenny, G., Fahey, C., . . . Morris, D. W.
825 (2014). Excess of rare novel loss-of-function variants in synaptic genes in schizophrenia
826 and autism spectrum disorders. *Mol Psychiatry, 19*(8), 872-879.
827 doi:10.1038/mp.2013.127

828 Korematsu, K., & Redies, C. (1997). Expression of cadherin-8 mRNA in the developing mouse
829 central nervous system. *J Comp Neurol, 387*(2), 291-306.
830 Lin, Y. C., Frei, J. A., Kilander, M. B., Shen, W., & Blatt, G. J. (2016). A Subset of Autism-
831 Associated Genes Regulate the Structural Stability of Neurons. *Front Cell Neurosci, 10*,
832 263. doi:10.3389/fncel.2016.00263
833 Manabe, T., Togashi, H., Uchida, N., Suzuki, S. C., Hayakawa, Y., Yamamoto, M., . . . Chisaka,
834 O. (2000). Loss of cadherin-11 adhesion receptor enhances plastic changes in
835 hippocampal synapses and modifies behavioral responses. *Mol Cell Neurosci, 15*(6), 534-
836 546. doi:10.1006/mcne.2000.0849
837 Marshall, C. R., Noor, A., Vincent, J. B., Lionel, A. C., Feuk, L., Skaug, J., . . . Scherer, S. W.
838 (2008). Structural variation of chromosomes in autism spectrum disorder. *Am J Hum*
839 *Genet, 82*(2), 477-488. doi:10.1016/j.ajhg.2007.12.009
840 Meijering, E., Jacob, M., Sarria, J. C., Steiner, P., Hirling, H., & Unser, M. (2004). Design and
841 validation of a tool for neurite tracing and analysis in fluorescence microscopy images.
842 *Cytometry A, 58*(2), 167-176. doi:10.1002/cyto.a.20022
843 Morrow, E. M., Yoo, S. Y., Flavell, S. W., Kim, T. K., Lin, Y., Hill, R. S., . . . Walsh, C. A.
844 (2008). Identifying autism loci and genes by tracing recent shared ancestry. *Science,*
845 *321*(5886), 218-223. doi:10.1126/science.1157657
846 Nahidiazar, L., Agronskaia, A. V., Broertjes, J., van den Broek, B., & Jalink, K. (2016).
847 Optimizing Imaging Conditions for Demanding Multi-Color Super Resolution
848 Localization Microscopy. *PLoS One, 11*(7), e0158884.
849 doi:10.1371/journal.pone.0158884
850 Nakanishi, M., Nomura, J., Ji, X., Tamada, K., Arai, T., Takahashi, E., . . . Takumi, T. (2017).
851 Correction: Functional significance of rare neuroligin 1 variants found in autism. *PLoS*
852 *Genet, 13*(10), e1007035. doi:10.1371/journal.pgen.1007035
853 Neale, B. M., Kou, Y., Liu, L., Ma'ayan, A., Samocha, K. E., Sabo, A., . . . Daly, M. J. (2012).
854 Patterns and rates of exonic de novo mutations in autism spectrum disorders. *Nature,*
855 *485*(7397), 242-245. doi:10.1038/nature11011
856 Nestor, M. W., Jacob, S., Sun, B., Prè, D., Sproul, A. A., Hong, S. I., . . . Noggle, S. A. (2015).
857 Characterization of a subpopulation of developing cortical interneurons from human
858 iPSCs within serum-free embryoid bodies. *Am J Physiol Cell Physiol, 308*(3), C209-219.
859 doi:10.1152/ajpcell.00263.2014
860 Noel, J., Ralph, G. S., Pickard, L., Williams, J., Molnar, E., Uney, J. B., . . . Henley, J. M.
861 (1999). Surface expression of AMPA receptors in hippocampal neurons is regulated by
862 an NSF-dependent mechanism. *Neuron, 23*(2), 365-376.
863 O'Roak, B. J., Vives, L., Girirajan, S., Karakoc, E., Krumm, N., Coe, B. P., . . . Eichler, E. E.
864 (2012). Sporadic autism exomes reveal a highly interconnected protein network of de
865 novo mutations. *Nature, 485*(7397), 246-250. doi:10.1038/nature10989
866 Osterhout, J. A., Josten, N., Yamada, J., Pan, F., Wu, S. W., Nguyen, P. L., . . . Huberman, A. D.
867 (2011). Cadherin-6 mediates axon-target matching in a non-image-forming visual circuit.
868 *Neuron, 71*(4), 632-639. doi:10.1016/j.neuron.2011.07.006
869 Ovesný, M., Křížek, P., Borkovec, J., Svindrych, Z., & Hagen, G. M. (2014). ThunderSTORM: a
870 comprehensive ImageJ plug-in for PALM and STORM data analysis and super-resolution
871 imaging. *Bioinformatics, 30*(16), 2389-2390. doi:10.1093/bioinformatics/btu202
872 Pagnamenta, A. T., Khan, H., Walker, S., Gerrelli, D., Wing, K., Bonaglia, M. C., . . . Monaco,
873 A. P. (2011). Rare familial 16q21 microdeletions under a linkage peak implicate cadherin

874 8 (CDH8) in susceptibility to autism and learning disability. *J Med Genet, 48*(1), 48-54.
875 doi:10.1136/jmg.2010.079426
876 Paradis, S., Harrar, D. B., Lin, Y., Koon, A. C., Hauser, J. L., Griffith, E. C., . . . Greenberg, M.
877 E. (2007). An RNAi-based approach identifies molecules required for glutamatergic and
878 GABAergic synapse development. *Neuron, 53*(2), 217-232.
879 doi:10.1016/j.neuron.2006.12.012
880 Phillips, A. W., Nestor, J. E., & Nestor, M. W. (2017). Developing HiPSC Derived Serum Free
881 Embryoid Bodies for the Interrogation of 3-D Stem Cell Cultures Using Physiologically
882 Relevant Assays. *J Vis Exp*(125). doi:10.3791/55799
883 Redies, C., Hertel, N., & Hübner, C. A. (2012). Cadherins and neuropsychiatric disorders. *Brain*
884 *Res, 1470*, 130-144. doi:10.1016/j.brainres.2012.06.020
885 Rubinson, D. A., Dillon, C. P., Kwiatkowski, A. V., Sievers, C., Yang, L., Kopinja, J., . . . Van
886 Parijs, L. (2003). A lentivirus-based system to functionally silence genes in primary
887 mammalian cells, stem cells and transgenic mice by RNA interference. *Nat Genet, 33*(3),
888 401-406. doi:10.1038/ng1117
889 Sanders, S. J., Ercan-Sencicek, A. G., Hus, V., Luo, R., Murtha, M. T., Moreno-De-Luca, D., . . .
890 State, M. W. (2011). Multiple recurrent de novo CNVs, including duplications of the
891 7q11.23 Williams syndrome region, are strongly associated with autism. *Neuron, 70*(5),
892 863-885. doi:10.1016/j.neuron.2011.05.002
893 Schulte, J. D., Srikanth, M., Das, S., Zhang, J., Lathia, J. D., Yin, L., . . . Chenn, A. (2013).
894 Cadherin-11 regulates motility in normal cortical neural precursors and glioblastoma.
895 *PLoS One, 8*(8), e70962. doi:10.1371/journal.pone.0070962
896 Seong, E., Yuan, L., & Arikkath, J. (2015). Cadherins and catenins in dendrite and synapse
897 morphogenesis. *Cell Adh Migr, 9*(3), 202-213. doi:10.4161/19336918.2014.994919
898 Song, J. Y., Ichtchenko, K., Südhof, T. C., & Brose, N. (1999). Neuroligin 1 is a postsynaptic
899 cell-adhesion molecule of excitatory synapses. *Proc Natl Acad Sci U S A, 96*(3), 1100-
900 1105.
901 Stan, A., Pielarski, K. N., Brigadski, T., Wittenmayer, N., Fedorchenko, O., Gohla, A., . . .
902 Gottmann, K. (2010). Essential cooperation of N-cadherin and neuroligin-1 in the
903 transsynaptic control of vesicle accumulation. *Proc Natl Acad Sci U S A, 107*(24), 11116-
904 11121. doi:10.1073/pnas.0914233107
905 Suzuki, S. C., Inoue, T., Kimura, Y., Tanaka, T., & Takeichi, M. (1997). Neuronal circuits are
906 subdivided by differential expression of type-II classic cadherins in postnatal mouse
907 brains. *Mol Cell Neurosci, 9*(5-6), 433-447. doi:10.1006/mcne.1997.0626
908 Takeichi, M., & Abe, K. (2005). Synaptic contact dynamics controlled by cadherin and catenins.
909 *Trends Cell Biol, 15*(4), 216-221. doi:10.1016/j.tcb.2005.02.002
910 van Harssel, J. J., Weckhuysen, S., van Kempen, M. J., Hardies, K., Verbeek, N. E., de Kovel, C.
911 G., . . . Brilstra, E. H. (2013). Clinical and genetic aspects of PCDH19-related epilepsy
912 syndromes and the possible role of PCDH19 mutations in males with autism spectrum
913 disorders. *Neurogenetics, 14*(1), 23-34. doi:10.1007/s10048-013-0353-1
914 Wang, C., Pan, Y. H., Wang, Y., Blatt, G., & Yuan, X. B. (2019). Segregated expressions of
915 autism risk genes Cdh11 and Cdh9 in autism-relevant regions of developing cerebellum.
916 *Mol Brain, 12*(1), 40. doi:10.1186/s13041-019-0461-4
917 Wang, K., Zhang, H., Ma, D., Bucan, M., Glessner, J. T., Abrahams, B. S., . . . Hakonarson, H.
918 (2009). Common genetic variants on 5p14.1 associate with autism spectrum disorders.
919 *Nature, 459*(7246), 528-533. doi:10.1038/nature07999

Willemsen, M. H., Fernandez, B. A., Bacino, C. A., Gerkes, E., de Brouwer, A. P., Pfundt, R., . . . Kleefstra, T. (2010). Identification of ANKRD11 and ZNF778 as candidate genes for autism and variable cognitive impairment in the novel 16q24.3 microdeletion syndrome. *Eur J Hum Genet, 18*(4), 429-435. doi:10.1038/ejhg.2009.192

Wu, N., Wang, Y., Pan, Y.-H., Yuan X. (2020). Identification of CDH11 as an ASD risk gene by matched-gene co-expression analysis and mouse behavioral studies. *bioRxiv* doi: 10.1101/2020.02.04.931121

Yamagata, M., Duan, X., & Sanes, J. R. (2018). Cadherins Interact With Synaptic Organizers to Promote Synaptic Differentiation. *Front Mol Neurosci, 11*, 142. doi:10.3389/fnmol.2018.00142

931 **Table 1. Primary and secondary antibodies.** Abbreviations: PSD-95, postsynaptic density
932 protein-95; GAT-1, sodium- and chloride-dependent GABA transporter-1; GAPDH,
933 glyceraldehyde 3-phosphate dehydrogenase; HRP, horseradish peroxidase; aa, amino acid; WB,
934 Western blot; ICC, immunocytochemistry; IP: Immunoprecipitation.

Primary						
Antibody	**Host, isotype**	**Immunogen**	**Source**	**Cat #**	**Clone no./RRID**	**Dilution**
Cadherin-8	Mouse	N-terminus, Mouse	DSHB	CAD8-1	RRID:AB_2078272	0.5 µg/mL (WB), 3-4 µg/mL (ICC), 2 µg (IP)
Cadherin-8	Goat, IgG	C-terminus, Human	Santa Cruz	sc-6461	C-18/RRID:AB_2078271	1:500
Cadherin-11	Mouse, IgG_1	C-terminus, Human	Thermo Fisher Scientific	32-1700	5B2H5/RRID:AB_2533068	2 µg/mL (WB), 7 µg (IP)
PSD-95	Mouse, IgG_{2a}	aa 77-299, Human	Neuro Mab	75-028	K28/43/RRID:AB_2307331	1:100,000 (WB)
PSD-95	Guinea pig, IgG	aa 64-247, Mouse	Synaptic Systems	124014	RRID:AB_2619800	1:500 (ICC)
Syntaxin-1	Mouse, IgG_{2a}	N-terminus, Rat	Synaptic Systems	110111	78.3/RRID:AB_887848	1:10,000
Synapsin-1	Rabbit, IgG	Native protein purified from bovine brain	Abgent	P17599	N/A	1:1000
GAT-1	Rabbit, IgG	C-terminus, Rat	Phospho Solutions	880-GAT1	RRID:AB_2492119	1:200
Neuroligin-1	Mouse, IgG_1	aa 718-843, Rat	Neuro Mab	75-160	N97A/31/RRID:AB_2235964	1:100
N-cadherin	Mouse, IgG_1	aa 802-819, Mouse	BD Transduction Labs	610920	32/RRID:AB_2077527	1:1000
β-catenin	Mouse, IgG_1	aa 571-781, Mouse	BD Transduction Labs	610153	14/RRID:AB_397554	1:700
Gephryin	Mouse, IgG_1	aa 326-550, Rat	Synaptic Systems	147111	3B11/RRID:AB_887719	1:1000
GAPDH	Rabbit, IgG	C-terminus, Human	Cell Signaling Technology	5174	D16H11/RRID:AB_10622025	1:1000
β-actin	Mouse, IgG_{2a}	N-terminus	Millipore Sigma	A5316	AC-74/RRID:AB_476743	1:5000

HA	Rabbit, IgG	aa 98-106 of human influenza hemagglutinin	Millipore Sigma	H6908	RRID:AB_260070	1:1000 (WB,) 1:25 (ICC), 4 µg (IP)
C-myc	Mouse, IgG_1	aa 408-439 of human $p62^{c\text{-}myc}$	Millipore Sigma	M4439	9E10/RRID:AB_291324	1:3000 (WB), 1:500 (ICC)
Flag	Mouse, IgG_{2b}	DYKDDDDK tag	Thermo Fisher Scientific	MA191878	FG4R/ RRID:AB_1957945	1:500 (ICC)
Secondary						
Antibody	**Host, isotype**	**Immunogen**	**Source**	**Cat #**	**Clone no./RRID**	**Dilution**
anti-rabbit IgG, HRP conjugate	Goat, IgG	IgG Rabbit	Cell Signaling Technology	7074P2	RRID:AB_2099233	1:7500
anti-mouse IgG, HRP conjugate	Goat, IgG	IgG Mouse	Thermo Fisher Scientific	A16072	RRID:AB_2534745	1:5000
anti-goat IgG, HRP conjugate	Donkey, IgG	IgG Goat	Thermo Fisher Scientific	A15999	RRID:AB_2534673	1:5000
anti-mouse Alexa488	Donkey, IgG	IgG (H+L) Mouse	Thermo Fisher Scientific	A21202	RRID:AB_141607	1:1000
Anti-mouse Alexa647	Donkey, IgG	IgG (H+L) Mouse	Thermo Fisher Scientific	A31571	RRID:AB_162542	1:1000
anti-rabbit Alexa488	Donkey, IgG	IgG (H+L) Rabbit	Thermo Fisher Scientific	A21206	RRID:AB_2535792	1:1000
anti-rabbit Alexa568	Donkey, IgG	IgG (H+L) Rabbit	Thermo Fisher Scientific	A10042	RRID:AB_2534017	1:1000
anti-rabbit Alexa647	Donkey, IgG	IgG (H+L) Rabbit	Thermo Fisher Scientific	A31573	RRID:AB_2536183	1:1000
anti-guinea pig Alexa488	Donkey, IgG	IgG (H+L) Guinea Pig	Jackson Immuno Research	706545148	RRID:AB_2340472	1:1000
anti-guinea pig Alexa568	Goat, IgG	IgG (H+L) Guinea Pig	Thermo Fisher Scientific	A11075	RRID:AB_2534119	1:1000

935

936 **Table 2. Case information of control and autism-derived iPSC lines.** Sample identity number,
937 gender, diagnosis and affected genes are listed for each iPSC line analyzed. Data was obtained
938 from the Hussman Institute for Human Genomics at the University of Miami (Hussman et al.,
939 2011; Cukier et al., 2014).
940

	Sample ID	Gender	Diagnosis	Genes
Autism	110	M	Autism	*VPS13B, EFCAB5, TRIM55*
	700	M	Autism	*RBFOX1*
	725	M	Autism	*CEP290, NINL, SOS2, TRIM55, ZMYND17, BTN2A2, MDC1, FBXO40, KIAA1949, SLC8A3, TSPYL5*
	732	M	Autism	*CLCN2, F13A1, JARID2, STXBP5, C12orf73, C20orf118, FGD6*
	134	M	Autism	*CPZ, PRICKLE1, TOPOR5*
	691	M	Autism	*COL6A3, SLIT3, C2orf85, AB13BP, UIMC1*
	709	M	Autism (Twin)	*RBFOX1*
	710	M	Autism (Twin)	*RBFOX1*
Control	574	M	-	-
	321	M	-	-
	322	M	-	-
	324	M	-	-

Figure Legends

Figure 1. Cadherin-8 and cadherin-11 show similar temporal and spatial expression patterns. (A) Temporal expression profile of cadherin-8 and cadherin-11 in mouse whole brain harvested at different developmental ages. Adult mice were 5 months old. **(B)** Line graph of temporal expression of the two cadherins. Values were normalized to P7. Cdh8: ****$p < 0.0001$, *$p = 0.046$ (P1), *$p = 0.0123$ (P21) compared to P7; Cdh11: *$p = 0.017$ (E14), *$p = 0.0296$ (adult) compared to P7; one-way ANOVA with Dunnett's multiple comparison test. N = 6 whole brains per age from three independent litters. Expression profiles of **(C)** cadherin-8 and **(D)** cadherin-11 in different brain areas, including cortex (CX), hippocampus (HC), cerebellum (CB) and thalamus/striatum (Th/St) at P14. **$p = 0.0048$ between CX and CB, *$p = 0.0259$ between HC and CB, *$p = 0.0326$ between CB and Th/St; one-way ANOVA with Tukey's multiple comparison test. N = 4 samples per brain area with 2-3 pooled brain areas per sample. Cadherin signals were normalized to GAPDH.

Figure 2. Cadherin-8 and cadherin-11 are enriched in postsynaptic densities and cadherin-8 interacts with neuroligin-1. (A) Forebrain tissues were subjected to synaptic fractionation analysis to determine the subcellular localization of cadherin-8 and cadherin-11. Markers (PSD-95 and syntaxin-1) were probed as control for purity of the fractionation. Total: total protein input, P1: nuclear, S1: cytosol/membranes, P2: crude synaptosome, S2: cytosol/light membranes, P3: synaptosome, SPM: synaptic plasma membrane, PSD: postsynaptic density, S3: synaptic vesicles. **(B)** Quantification of protein enrichment in SPM and PSD fractions compared to total protein input. PSD-95: **$p = 0.0012$ between SPM and total, ****$p < 0.0001$ between PSD and total, *$p = 0.0444$ between SPM and PSD; Cdh8: *$p = 0.0332$ between PSD and total; Cdh11: **$p = 0.0039$ between SPM and total, ***$p = 0.0002$ between PSD and total; one-way ANOVA with Tukey's multiple comparison test. N = 8 P21 mice, two pooled forebrains per sample. Immunoprecipitation (IP) of **(C)** cadherin-8 and **(D)** cadherin-11 from P14 forebrain tissues. β-catenin signal is detectable in the IP of cadherin-8 and cadherin-11 and neuroligin-1 signal is detectable in the IP of cadherin-8. **(E)** Immunocytochemistry of N2a cells over-expressing cadherin-8-myc (magenta) and neuroligin-1-HA (cyan), counterstained for DAPI (blue). Cadherin-8-myc and neuroligin-1-HA show partial co-localization at cell-cell contacts (arrowheads) and at the cell membrane (open arrowheads). Boxed areas are magnified. Scale bar = 20 µm.

Figure 3. Cadherin-8 localizes to excitatory synapses. Representative confocal images showing surface expressed cadherin-8 (cyan) on dendritic segments of cultured hippocampal neurons at 15 DIV co-immunostained with either the excitatory synaptic markers **(A)** PSD-95 (magenta) and synapsin-1 (yellow), or the inhibitory synaptic marker **(B)** GAT-1 (magenta). Cadherin-8 puncta co-localizing with PSD-95- or GAT-1-positive puncta (open arrowheads), being adjacent to PSD-95- or GAT-1-positive puncta (arrowheads) and PSD-95- or GAT-1-negative cadherin-8 puncta (arrows) were analyzed. Scale bar = 2 µm. Representative synaptic puncta are magnified (boxed areas, scale bar = 1 µm). The synaptic profile of cadherin-8-positive puncta were quantified and analyzed as fractions of co-localization with **(C)** PSD-95 or **(D)** GAT-1. PSD-95: **$p = 0.0019$, co-localization with PSD-95 versus adjacent to PSD-95; ***$p = 0.002$, adjacent to PSD-95 versus PSD-95-negative puncta; GAT-1: ****$p < 0.0001$, comparison between all fractions; one-way ANOVA with Tukey's multiple comparison test. N = 11-14 neurons, three independent cultures. dSTORM imaging was performed on 15 DIV hippocampal neurons immunostained for PSD-95 (magenta) and either surface-expressed **(E)** cadherin-8 (cyan) or **(F)** neuroligin-1 (cyan). Scale bar: 5 µm. Insets (800 nm) show 3D proximity of PSD-95 to the surface stained proteins. Crosshair

shows YZ and XZ planes. **(G-J)** Nearest neighbor analysis of dSTORM data. Individual surface stained **(G)** cadherin-8 and **(H)** neuroligin-1 puncta were isolated, and the nearest PSD-95 puncta was determined. **(I)** Quantification and comparison of nearest neighbor analysis for cadherin-8, neuroligin-1 and a randomized set of numbers generated between 0-400 nm. **(J)** Quantification and comparison of the frequency distribution of cadherin-8 and neuroligin-1 puncta and a randomized data set between 0 and 50 nm from the nearest PSD-95 puncta. ***$p = 0.0001$, ****$p < 0.0001$; one-way ANOVA with Tukey's multiple comparison test. N = 23 neurons (Cdh8) and 19 neurons (Nlgn1), 18 random data points, three independent cultures. 50 particles per cell were used, unless fewer particles were available.

Figure 4. **Elevated cadherin-8 expression in *Cdh11*$^{-/-}$ mice is accompanied by an increase of excitatory synaptic proteins and dendrite complexity. (A)** Western blot analysis of the expression levels of cadherin-11 and cadherin-8 in P7 *Cdh11* wild-type (WT), heterozygous (HZ) and knockout (KO) mouse brains. Cadherin-11 expression is not detectable in *Cdh11* KO brains. Cadherin signals were normalized to GAPDH. Quantification of the expression of **(B)** cadherin-11 and **(C)** cadherin-8 in *Cdh11* WT, HZ and KO brains. Cdh11: ****$p < 0.0001$, KO vs WT and KO vs HZ; ***$p = 0.0002$, HZ vs WT; Cdh8: *$p = 0.0399$, KO vs WT; *$p = 0.0143$, KO vs HZ; one-way ANOVA with Tukey's multiple comparison test. N = 7 animals per genotype. **(D)** Western blot analysis of the expression profiles of neuroligin-1, PSD-95 and gephyrin in P7 *Cdh11* WT and KO mouse brains. Signals were normalized to β-actin. Quantification of the expression of **(E)** neuroligin-1, **(F)** PSD-95 and **(G)** gephyrin in *Cdh11* WT and KO brains. Nlgn1: **$p = 0.027$; PSD95: **$p = 0.0022$; unpaired two-tailed *t*-test. N = 12 WT and 11 KO animals. **(H)** Confocal fluorochrome images of dendritic spines from primary, secondary and tertiary dendrites from 15 DIV *Cdh11* WT and KO hippocampal neurons transfected with pLL3.7-GFP. Scale bar = 2 µm. **(I)** Quantification of the mean spine density of 15 DIV *Cdh11* WT and KO hippocampal neurons. N = 33 WT and 28 KO neurons. **(J)** Representative images of reconstructed dendritic trees from 15 DIV *Cdh11* WT and KO hippocampal neurons. Scale bar = 100 µm. **(K)** Sholl analysis of reconstructed neurons. Significant difference was determined by quantifying the area under the Sholl curve (AUC) between WT and KO neurons; *$p = 0.0269$, unpaired two-tailed *t*-test. N = 23 WT and 25 KO neurons. Quantification of **(L)** total dendrite length and **(M)** branch tip number of *Cdh11* WT and KO neurons. (L) *$p = 0.0323$; (M) *$p = 0.0212$; unpaired two-tailed *t*-test. N = 23 WT and 25 KO neurons.

Figure 5. *Cdh11*$^{-/-}$ mice show altered calcium activity and miniature excitatory postsynaptic currents. (A) Example calcium current traces from *Cdh11* wild-type (WT) and *Cdh11* knockout (KO) hippocampal cultures at 15 DIV recorded for 3 minutes using NeuroBurst Orange lentivirus calcium indicator. Averaged fluorescence intensity per cell of 1940 active neurons (WT) and 1009 active neurons (KO) was plotted against time (sec). Measurement of **(B)** number of active neurons, **(C)** correlation of activity **(D)** mean burst strength and **E)** mean burst rate of *Cdh11* WT and KO hippocampal neurons recorded at 15 DIV and 16 DIV. *$p = 0.0160$, **$p = 0.0049$, ***$p = 0.0006$; unpaired two-tailed *t*-test. N = 6 WT and 7 KO cultures from two different time points. **(F)** Example current traces recorded from whole-cell voltage-clamp of hippocampal CA1 pyramidal neurons. **(G)** Examples of average (left) and scaled (right) mEPSC traces from *Cdh11* WT and KO cells. Measurement of **(H)** frequency, **(I)** amplitude, **(J)** charge, **(K)** rise time and **(L)** decay time constant of recorded mEPSCs. ****$p > 0.0001$, *$p = 0.0166$; unpaired two-tailed *t*-test. N = 25 WT and 23 KO neurons.

Figure 6. iPSC-derived cortical NPCs and organoids from autistic individuals show altered expression of CDH8 and CDH11. Western blot analysis and quantification of **(A)** CDH8 and **(B)** CDH11 expression in iPSC-derived cortical NPCs from typically-developing control and autistic individuals at 19 DIV. Quantification of the expression of each cadherin is represented as bar graph and as box and whisker plot. $^{**}p = 0.0027$, $^{*}p = 0.0323$; unpaired two-tailed *t*-test. N = 4 control and 8 autistic individuals, triplicates of each individual. Cadherin signals were normalized to GAPDH. Quantification of mRNA expression of **(C)** CDH8 and **(D)** CDH11 in cortical organoids derived from iPSCs of control and autistic individuals at 60 DIV via qPCR. $^{*}p = 0.0473$, $^{***}p = 0.0001$; unpaired two-tailed *t*-test. N = 4 control and 6 autism individuals, triplicates of each individual.

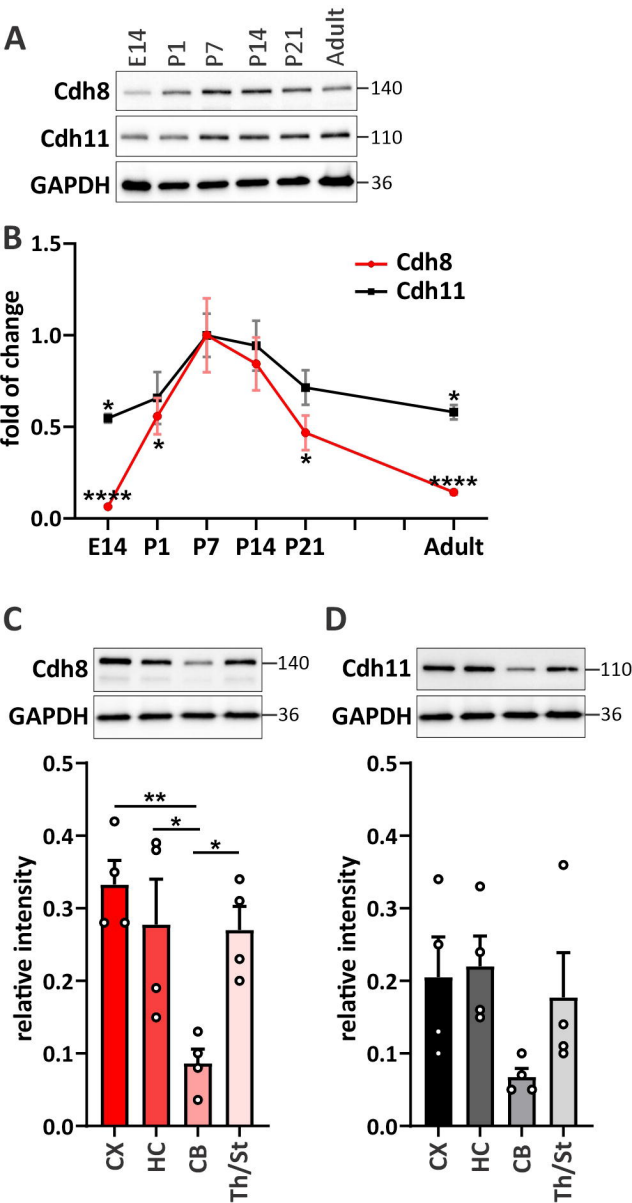
A
E14
P1
P7
P14
P21
Adult
Cdh8
Cdh11
GAPDH
140
110
36
B
fold of change
Cdh8
Cdh11
1.5
1.0
0.5
0.0
****
*
*
*
*
****
E14
P1
P7
P14
P21
Adult
C
Cdh8
GAPDH
140
36
relative intensity
**
*
*
CX
HC
CB
Th/St
D
Cdh11
GAPDH
110
36
relative intensity
CX
HC
CB
Th/St

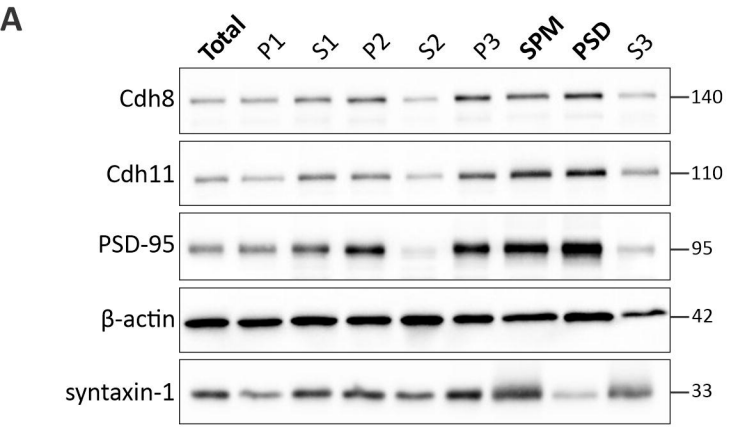

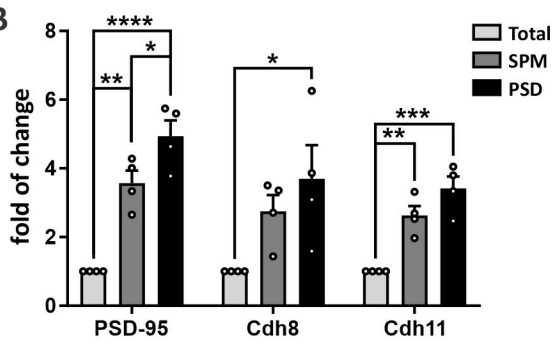

	Enrichment in SPM	Enrichment in PSD
PSD-95	3.6 (± 0.36)	4.9 (± 0.46)
Cdh8	2.8 (± 0.47)	3.7 (± 0.97)
Cdh11	2.6 (± 0.71)	3.4 (± 0.88)

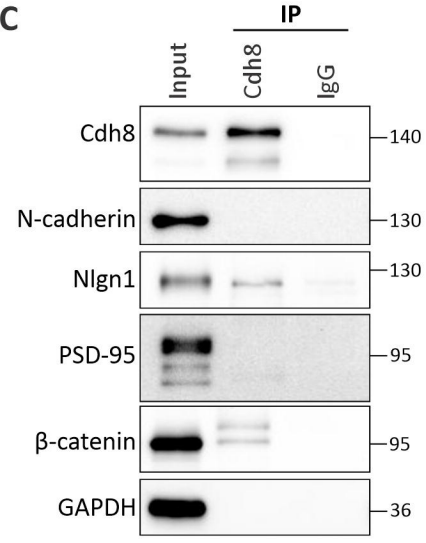

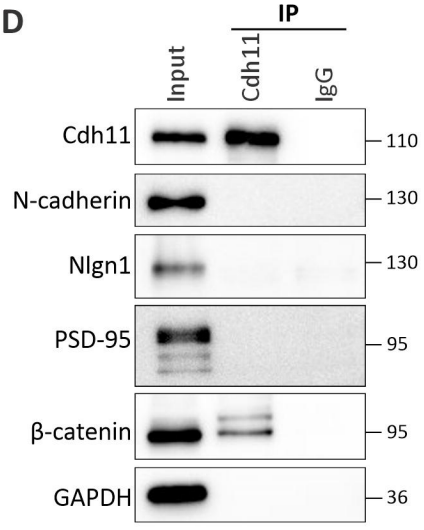

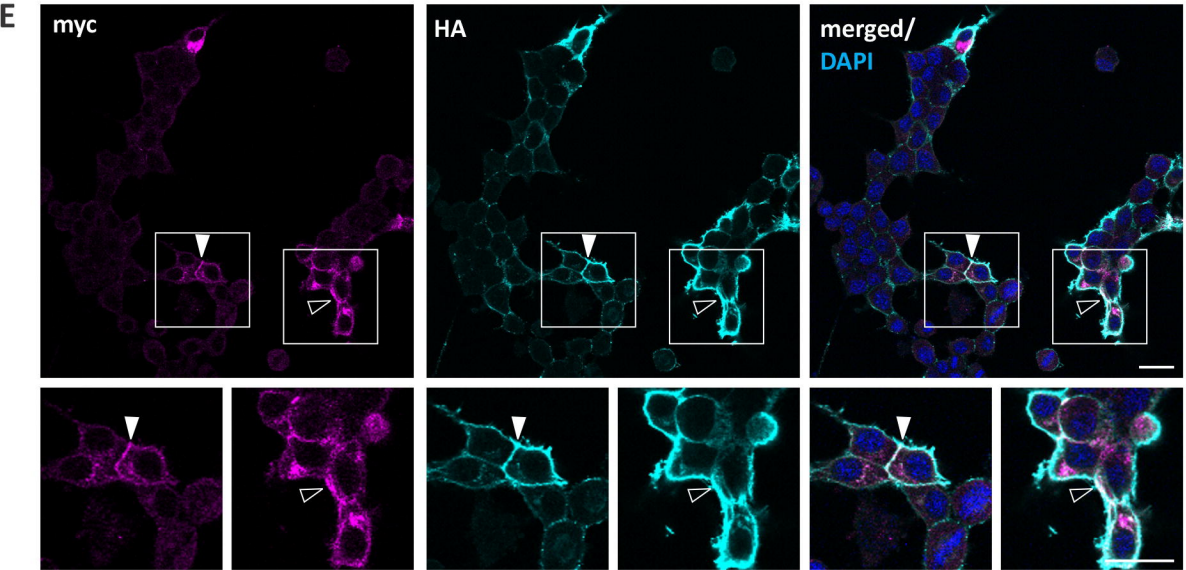

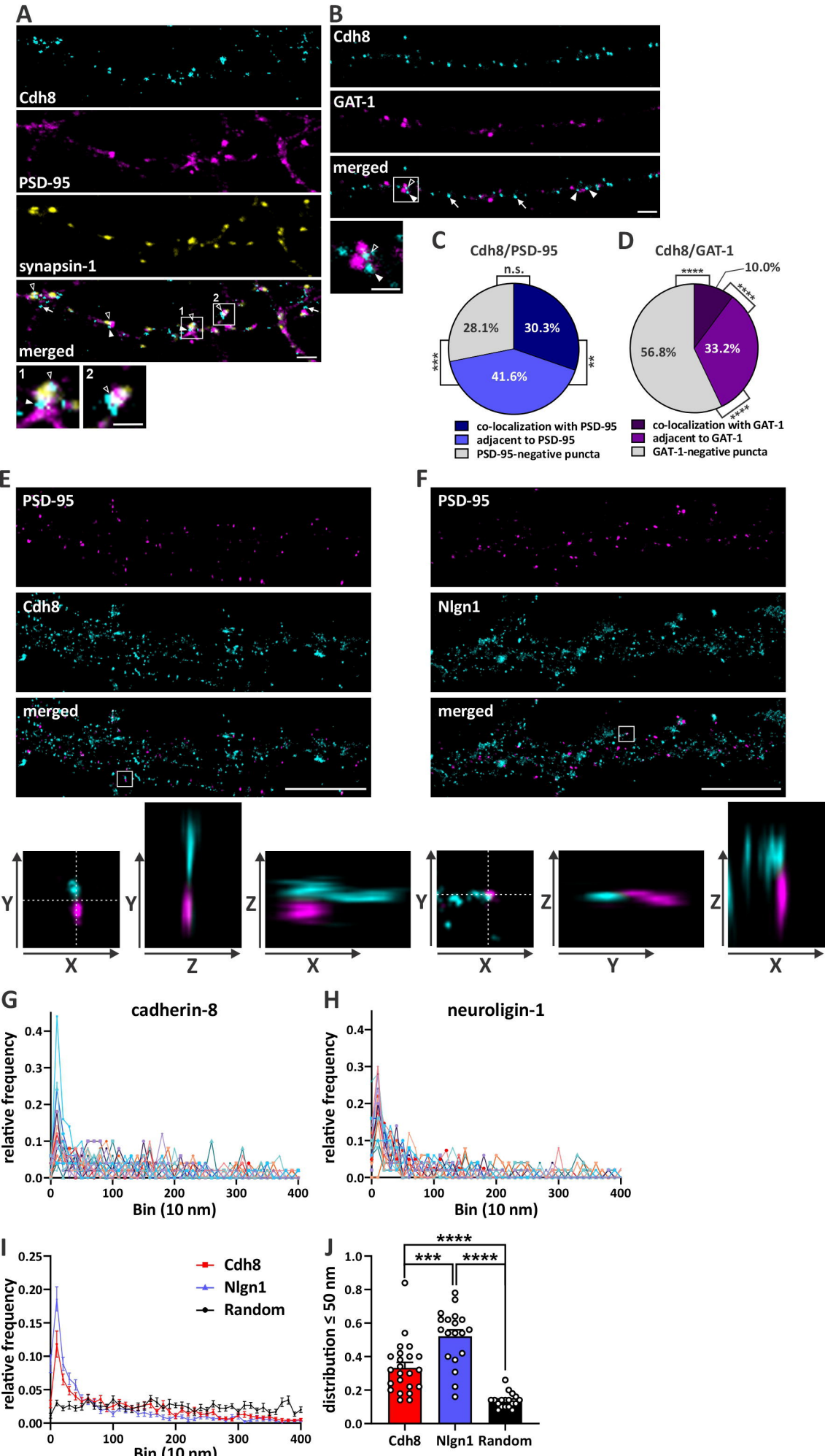
A
Cdh8
PSD-95
synapsin-1
merged
1
2
B
Cdh8
GAT-1
merged
C
Cdh8/PSD-95
n.s.
30.3%
41.6%
28.1%
**
***
co-localization with PSD-95
adjacent to PSD-95
PSD-95-negative puncta
D
Cdh8/GAT-1
****
10.0%
33.2%
56.8%
co-localization with GAT-1
adjacent to GAT-1
GAT-1-negative puncta
E
PSD-95
Cdh8
merged
F
PSD-95
Nlgn1
merged
Y
X
Z
G
cadherin-8
relative frequency
Bin (10 nm)
H
neuroligin-1
relative frequency
Bin (10 nm)
I
Cdh8
Nlgn1
Random
relative frequency
Bin (10 nm)
J
****
***
****
distribution ≤ 50 nm
Cdh8
Nlgn1
Random

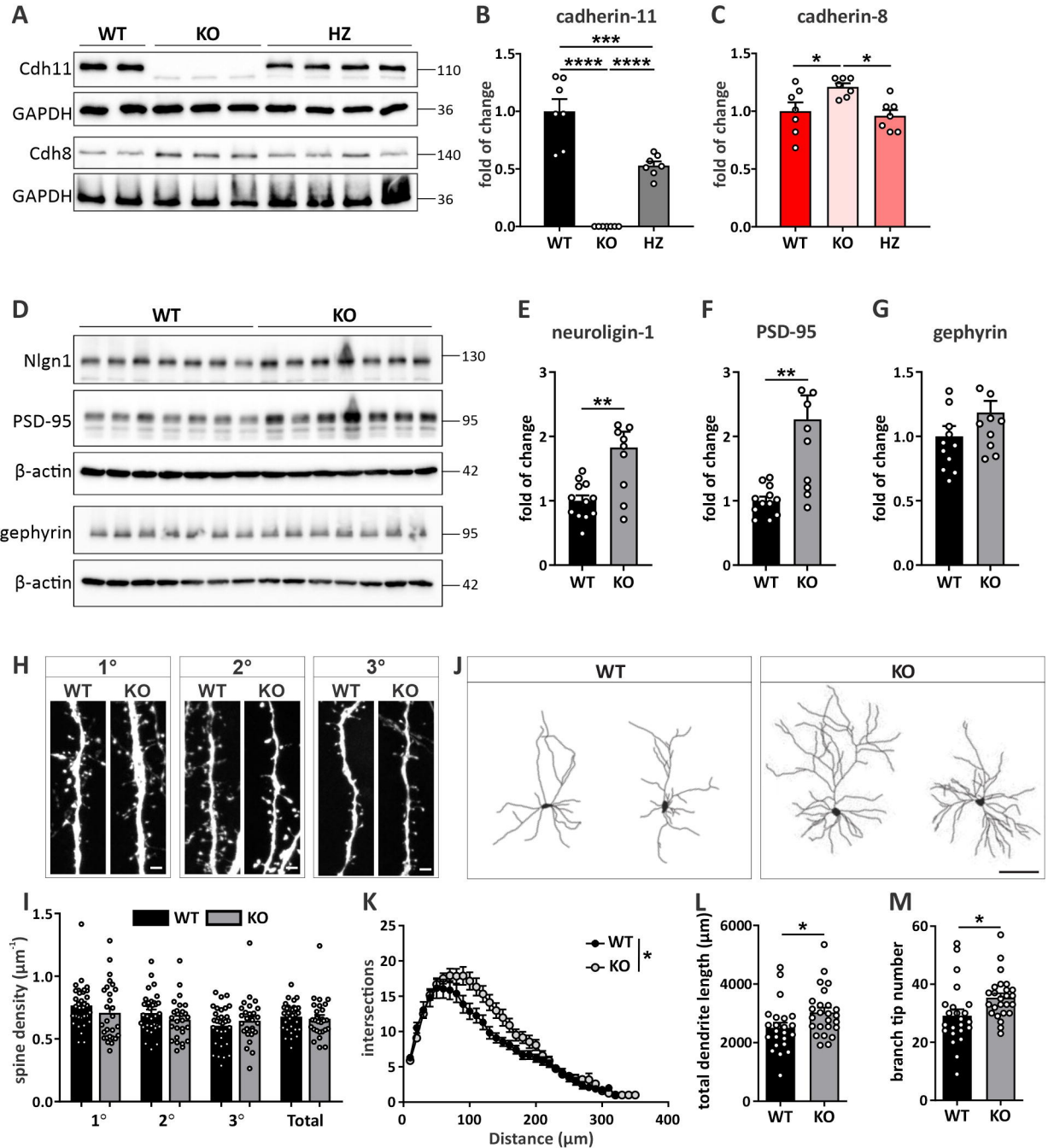
A
WT
KO
HZ
Cdh11
GAPDH
Cdh8
GAPDH
110
36
140
36
B
cadherin-11
fold of change
WT
KO
HZ
C
cadherin-8
fold of change
WT
KO
HZ
D
WT
KO
Nlgn1
PSD-95
β-actin
gephyrin
β-actin
130
95
42
95
42
E
neuroligin-1
fold of change
WT
KO
F
PSD-95
fold of change
WT
KO
G
gephyrin
fold of change
WT
KO
H
1°
2°
3°
WT
KO
J
WT
KO
I
WT
KO
spine density (µm-1)
1°
2°
3°
Total
K
WT
KO
intersections
Distance (µm)
L
total dendrite length (µm)
WT
KO
M
branch tip number
WT
KO

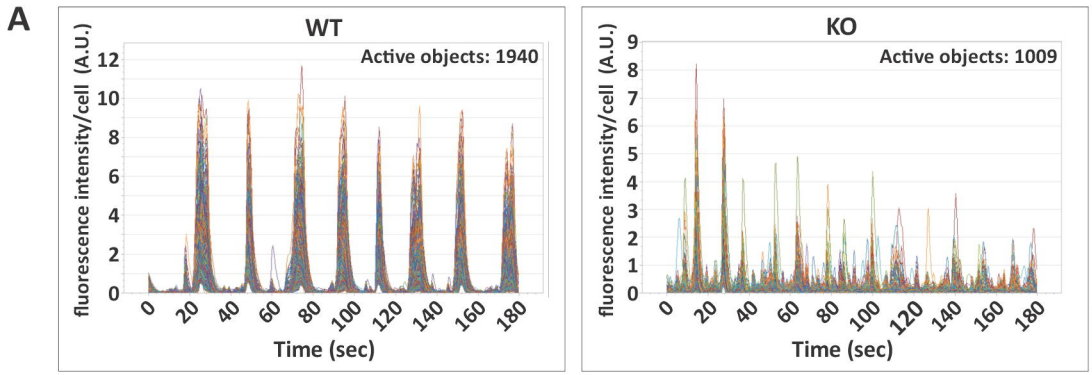
A
WT
Active objects: 1940
fluorescence intensity/cell (A.U.)
Time (sec)
KO
Active objects: 1009
fluorescence intensity/cell (A.U.)
Time (sec)

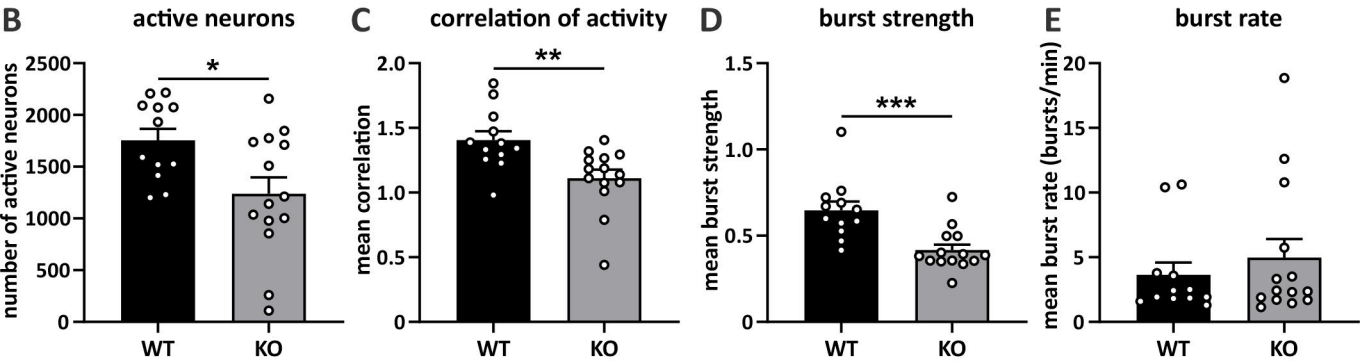
B
active neurons
number of active neurons
WT
KO
C
correlation of activity
mean correlation
D
burst strength
mean burst strength
E
burst rate
mean burst rate (bursts/min)

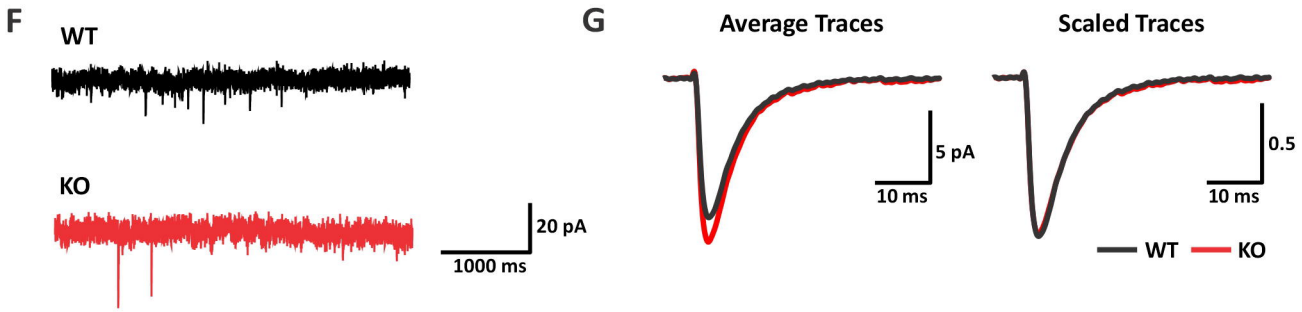
F
WT
KO
20 pA
1000 ms
G
Average Traces
Scaled Traces
5 pA
10 ms
0.5
10 ms
WT
KO

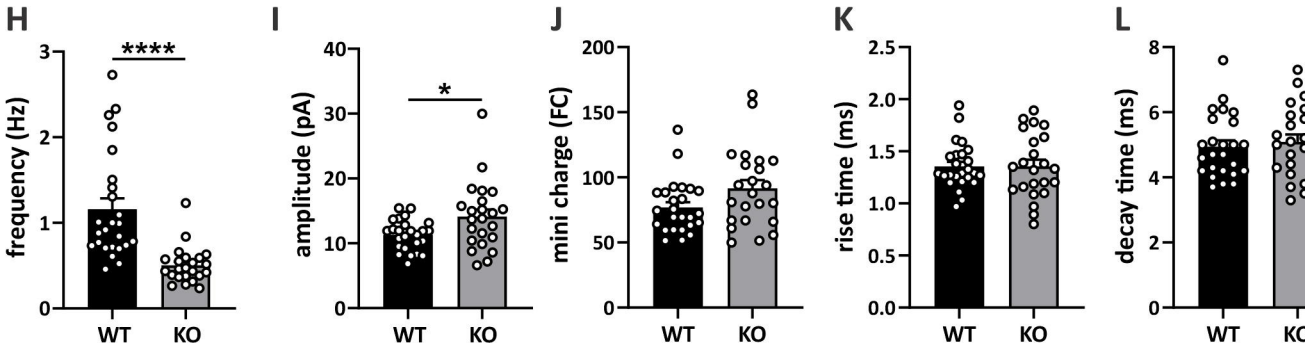
H
frequency (Hz)
I
amplitude (pA)
J
mini charge (FC)
K
rise time (ms)
L
decay time (ms)
WT
KO

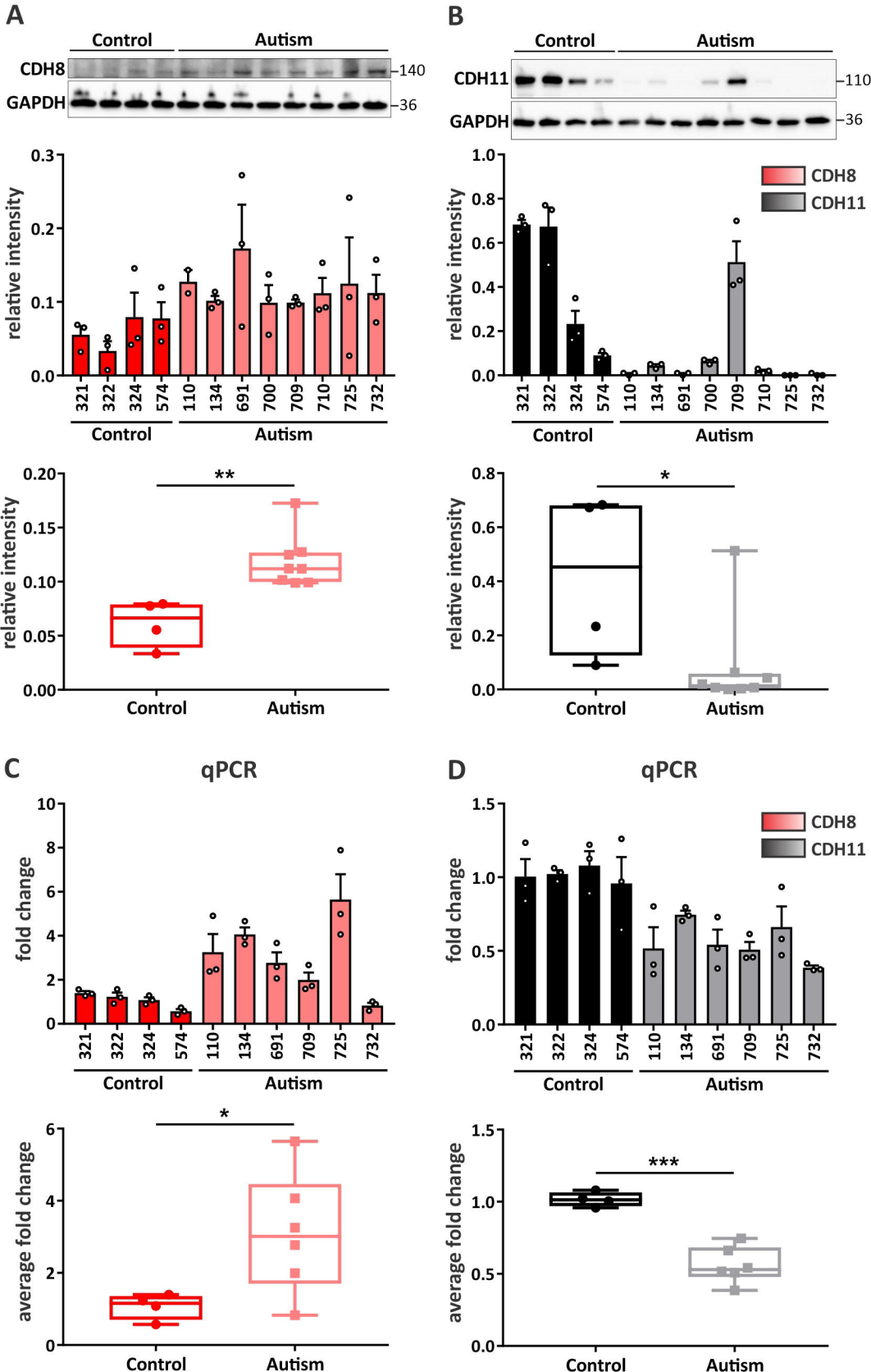
A
Control
Autism
CDH8
GAPDH
140
36
relative intensity
0.3
0.2
0.1
0.0
321
322
324
574
110
134
691
700
709
710
725
732
Control
Autism
**
0.20
0.15
0.10
0.05
0.00
Control
Autism
B
Control
Autism
CDH11
GAPDH
110
36
relative intensity
1.0
0.8
0.6
0.4
0.2
0.0
CDH8
CDH11
321
322
324
574
110
134
691
700
709
710
725
732
Control
Autism
*
0.8
0.6
0.4
0.2
0.0
Control
Autism
C
qPCR
fold change
10
8
6
4
2
0
321
322
324
574
110
134
691
709
725
732
Control
Autism
*
average fold change
6
4
2
0
Control
Autism
D
qPCR
fold change
1.5
1.0
0.5
0.0
CDH8
CDH11
321
322
324
574
110
134
691
709
725
732
Control
Autism
***
average fold change
1.5
1.0
0.5
0.0
Control
Autism